Determining the Function of Myo1p: a Novel, Unconventional Myosin in *Tetrahymena thermophila*

by

Selwyn A. Williams

A dissertation submitted to the Graduate Faculty in Biology in partial fulfillment of the requirements for the degree of Doctor of Philosophy, The City University of New York.

2004

Reproduced with permission of the copyright owner. Further reproduction prohibited without permission.

UMI Number: 3144151

INFORMATION TO USERS

The quality of this reproduction is dependent upon the quality of the copy submitted. Broken or indistinct print, colored or poor quality illustrations and photographs, print bleed-through, substandard margins, and improper alignment can adversely affect reproduction.

In the unlikely event that the author did not send a complete manuscript and there are missing pages, these will be noted. Also, if unauthorized copyright material had to be removed, a note will indicate the deletion.

UMI®

UMI Microform 3144151

Copyright 2004 by ProQuest Information and Learning Company.

All rights reserved. This microform edition is protected against unauthorized copying under Title 17, United States Code.

ProQuest Information and Learning Company
300 North Zeeb Road
P.O. Box 1346
Ann Arbor, MI 48106-1346

Reproduced with permission of the copyright owner. Further reproduction prohibited without permission.

This manuscript has been read and accepted for the Graduate Faculty in Biology in satisfaction of the dissertation requirement for the degree of Doctor of Philosophy.

May 28, 2004
Date

Chair of Examining Committee,
Dr. Ray H. Gavin, Brooklyn College

June 1, 2004
Date

Executive Officer,
Dr. Richard L. Chappell

Dr. Dan Eshel, Brooklyn College

Dr. Theodore Muth, Brooklyn College

Dr. William Cohen, Hunter College

Dr. Derrick Brazill, Hunter College

Dr. Phillip Davies, Merck Research Laboratories

Supervising Committee

The City University of New York

Reproduced with permission of the copyright owner. Further reproduction prohibited without permission.

Abstract

Determining the Function of Myo1p: A Novel, Unconventional Myosin in *Tetrahymena thermophila*

by

Selwyn A. Williams

Adviser: Dr. Ray H. Gavin

In an earlier study (Garces et al. 1998), *MYO1* and its encoded product, Myo1p, were identified by a PCR-based genomic screen of the ciliate protozoan, *Tetrahymena thermophila*. Head domain homology analysis based on partial genomic sequence data, phylogenetically defined Myo1p as a novel, unconventional myosin heavy chain, not belonging to any of the previously established myosin classes. In the present study, a Basic Local Alignment Search Tool (BLAST) analysis of a searchable database created by the *Tetrahymena* Genome Project was used to determine the complete genomic sequence of *MYO1* and to predict the structure of Myo1p. *MYO1* is a 7 kb gene encoding a ~2000 aa-heavy chain polypeptide. Myo1p is predicted to have a 300 aa-N-terminal extension, a 750 aa-conserved motor domain, two IQ motifs, and 190 aa-FERM domain located 250-300 residues from the C-terminal end of the protein. Phenotypic analysis of a *MYO1*-knockout (Δ*MYO1*) strain revealed temperature dependent defects in macronuclear elongation and endocytosis. In dividing knockout cells at 20 ^{0}C, the macronucleus failed to elongate properly along the anterior-posterior axis resulting in

Reproduced with permission of the copyright owner. Further reproduction prohibited without permission.

grossly unequal nuclear segregation. At 20 ^{0}C, *MYO1*-knockout cells also exhibited reduced rates of food vacuole formation when compared with wild-type. A *Tetrahymena* strain expressing GFP-actin showed fusion-protein localization to cortical structures (basal body cage) and the contractile ring. Incorporation of GFP-actin into filament-associated structures resulted in the temperature-dependent impairment of macronuclear elongation (phenotypically similar to Δ*MYO1*) and cytokinesis. Anti-actin immunolocalization studies demonstrated that actin was closely associated with nascent food vacuoles in the oral regions of both wild-type and *MYO1*-knockout cells. Electron microscopy, however, revealed significant differences in vacuole morphology between wild-type and *MYO1*-knockout *Tetrahymena.* Wild type cells possessed vacuoles that were rapidly expanded through membrane fusions, whereas *MYO1*-knockout cells accumulated comparatively smaller nascent food vacuoles. These accumulations frequently formed multi-vacuolar aggregates comprised of clusters of small vacuoles loosely connected by slender vacuolar extensions. The evidence presented in this study suggests that an actin-Myo1p contractile system may have a novel function within the cell apparatus facilitating macronuclear division, and may also provide the translocatory component for rapid vacuole-vacuole fusion during early endosome expansion.

Reproduced with permission of the copyright owner. Further reproduction prohibited without permission.

Preface

Legend has it that when the great classical Greek mathematician, Archimedes, discovered the law of displacement which later became known as Archimedes Principle, he ran naked in the streets of Syracuse shouting, "Eureka! (I've got it)". During the production of this thesis, my mentor, my co-workers and I shared quite a few euphoric, "eurekan" moments in the lab, although we haven't (as yet) been caught streaking on campus! A special debt of gratitude is owed to my senior colleagues, Roland Hosein, Phillip Solomon and Kester Haye, as well as all the participating undergraduates whose tireless innovations and efforts kept this project moving forward. To my peers and my professors at the Biology department of Brooklyn College, thank you for providing the robust intellectual milieu over the years that proved essential to my academic growth and development. I also wish to acknowledge the members of my Examination Committee: Drs. Dan Eshel, Theodore Muth, Derrick Brazill and Bill Cohen whose inquiries and suggestions contributed significantly to overall development of this thesis. A special thanks to Dr. Phil Davies for his remarkable dependability and guidance during the latter stages of this process. To Dr. Jorge Garces and Dr. Mike Menser, I am indebted to you for sharing with me your keen intuition and understanding of issues both personal and professional.

This body of work would not have possible without the unwavering support of my mother (who, I always remember, would accompany me to collect frogs and cockroaches for my high school biology class and constantly encouraged my interest in science), my

Reproduced with permission of the copyright owner. Further reproduction prohibited without permission.

siblings and friends who always cheered me on, and my loving (and extremely understanding) wife, Dianne.

And finally to my mentor, friend, and benefactor, Ray Gavin, who gave me the opportunity to become what I am today. Who would have thought that the project you assigned me as an undergraduate would eventually blossom into a dissertation thesis? Thank you for your astute tutelage, your dedicated friendship and your boundless generosity. I eagerly look forward to the day when I proudly explain to my young son, the person after whom he has been named. Thanks for the inspiration.

To the next generation of researchers: Darielle, Cadell, Caleb and Ray Jr.... stay curious!

Reproduced with permission of the copyright owner. Further reproduction prohibited without permission.

Table of Contents

Content	Page
Abstract	iii
Preface	v
Table of Contents	vii
List of Tables	viii
List of Figures	ix
Chapter 1 Introduction: Myosins	1
Chapter 2 Materials and Methods	9
Chapter 3 Determination of the Complete Sequence of *MYO1*	20
Chapter 4 A Genomic Knockout of *MYO1*	26
Chapter 5 Expression of GFP-Actin in *Tetrahymena*	34
Chapter 6 Immunological and Ultrastructural Evidence for the Roles of Actin and Myolp in the Endocytic Pathway	42
Chapter 7 Conclusions, Work in Progress and Future Directions	47
Bibliography	78

Reproduced with permission of the copyright owner. Further reproduction prohibited without permission.

List of Tables

Table	Page
Table 1 List of primers	52
Table 2 Uptake of latex beads by wild-type and Δ*MYO1 Tetrahymena thermophila*	53
Table 3 Macronuclear position in exponentially growing wild-type and Δ*MYO1 Tetrahymena thermophila*	54
Table 4 Division of macronuclear division stages in exponentially growing wild-type and Δ*MYO1 Tetrahymena thermophila*	55
Table 5 Immunogold localization of actin to basal bodies	56
Table 6 Morphometry of GFP-actin strain of *Tetrahymena thermophila*	57
Table 7 Morphometry of vacuole distribution	58

Reproduced with permission of the copyright owner. Further reproduction prohibited without permission.

List of Figures

Figure	Page
Fig. 1 An unrooted phylogenetic tree of the myosin superfamily	59
Fig. 2 The myosin classes	60
Fig. 3 Genomic clones and cDNA amplification products derived from library screens	61
Fig. 4 A map of *MYO1* and aligned preliminary contigs	62
Fig. 5 Verification of *MYO1* genomic contigs by PCR	63
Fig. 6 Open Reading Frames, domain structure, and RT-PCR of Myo1p	64
Fig. 7 A *MYO1* construct transformed *Tetrahymena thermophila*	65
Fig. 8 Morphometry of wild-type and Δ*MYO1* populations of *Tetrahymena thermophila* grown at 20 ^{0}C and 35 ^{0}C	66
Fig. 9 A diagrammatic representation of the stages in macronuclear division of the cell *Tetrahymena thermophila*	67
Fig. 10 DAPI-stained wild-type and *MYO1*-knockout (Δ*MYO1*) cells of *Tetrahymena thermophila* at 20 ^{0}C	68
Fig. 11 DAPI-stained Δ*MYO1* cells of *Tetrahymena thermophila* from cultures maintained at 20 ^{0}C	69
Fig. 12 Expression of actin and GFP-actin in *Tetrahymena*	70

Reproduced with permission of the copyright owner. Further reproduction prohibited without permission.

List of Figures (continued)

Figure	Page
Fig. 13 Confocal microscope images of *Tetrahymena thermophila* expressing GFP-actin in vivo	71
Fig. 14 Immunogold localization of actin	72
Fig. 15 Cells arrested in cytokinesis	73
Fig. 16 A diagrammatic representation of major steps in the endocytic pathway in *Tetrahymena thermophila*	74
Fig. 17 Actin immunolocalization to food vacuoles and cortical structures in *Tetrahymena*	75
Fig. 18 Transmission electron micrographs showing vacuole morphology in wild-type and Δ*MYO1 Tetrahymena thermophila*	76
Fig. 19 Conjectural models of Myo1p function in macronuclear elongation and vacuolar fusion	77

Reproduced with permission of the copyright owner. Further reproduction prohibited without permission.

CHAPTER 1

INTRODUCTION: MYOSINS

Myosins are complex enzymatic motors with the ability to generate unidirectional, chemomechanical force. Biochemically defined as actin-activated Mg^{2+}-ATPases (Cope et al. 1996), myosins catalyze an ATP-dependent interaction with actin microfilaments. This functionality resides in the ~80 kDa motor domain, almost exclusively found at the N-terminus, which is highly conserved among all myosins. In all known myosins the energy transducing head is coupled to additional domains. In most myosins, these additional domains are differentiated into a regulatory neck region and a tail. The head or motor domain contains both the ATP-binding site and the actin filament-binding site of the enzyme. The neck region of myosins contains a variable number of light chain binding sites known as IQ motifs and is often characterized by consensus sequence repeats (Mooseker and Cheney, 1995). It consists of a basic and hydrophobic 20-25 amino acid stretch that conforms to the sequence: IQxxxRGxxxRK (Mooseker and Cheney, 1995). The essential or regulatory light chains that associate with the IQ motifs include calcium-binding calmodulin and members of the EF-hand family of proteins. The neck region is thought to act as a "lever arm" that amplifies and originates the movement of the catalytic head domain (Spudich, 1994). Following the neck domain, most myosins possess a C-terminal tail region. In general, myosins within a given class or subclass share structurally similar tail domains. Highly divergent in structural and biochemical properties, myosin tails confer functional specialization to the motor by targeting the protein to a specific subcellular location or by promoting an interaction with

Reproduced with permission of the copyright owner. Further reproduction prohibited without permission.

other proteins and other cellular substrates. The tail motifs known to exist in various myosins include membrane-binding, actin-binding (GPA), coiled-coil, GTPase activation (Rho-GAP and Rho-GEF), Src homology 3 (SH3), zinc-finger, FERM, PDZ and pleckstrin homology (PH) domains, reflecting the diverse roles of these motors in cellular processes (Fig 2).

Conventional and Unconventional Myosins

Since its identification one hundred and forty years ago, muscle myosin has been extensively studied and characterized in its fudamental role in muscle contraction. This founding group was called myosin II because the multimeric complex included two dimerized heavy chain polypeptides. The tails of myosin II form extended alpha-helical coiled-coils that enable myosin assembly into bipolar filaments, and in cooperation with actin filaments, establish the sarcomeric lattice necessary for efficient force transduction in muscles (Cope et al. 1996). Conventional myosins, as they are also called, include the filament forming non-muscle myosin IIs which are essential for cytokinesis.

Purification of actin and myosin from the plasmodial slime mould *Physarum* (Adelman and Taylor, 1969a, 1969b) and the subsequent characterization of *Acanthamoeba* actin (Weihling and Korn 1971) spawned a new field of inquiry in cell biology. Discovery of the first single-headed, nonfilament forming, "mini" myosin in *Acanthamoeba* a few years later (Pollard and Korn 1973) quickly solidified interest in nonmuscle contractile proteins. Later termed *unconventional* myosins, the nonfilament-forming myosins added complexity and diversity to the emerging new field. In recent years, the discovery of new myosins in evolutionarily diverse organisms has flourished and unconventional myosins now encompass a superfamily of proteins with highly

Reproduced with permission of the copyright owner. Further reproduction prohibited without permission.

conserved N-terminal domains, but with C-termini unlike those of conventional myosins (Fig. 2)

Structure of the Motor Domain

Skeletal muscle myosin II subfragment 1 (S1) has been used as a prototype for various studies of myosin head domain structure. Limited proteolytic digestion of S1 has revealed three domains from N terminus to C terminus: 25, 50, and 20 kDa. The sites for this proteolytic digestion are located within surface loops that are susceptible to enzymatic digestion as revealed by the atomic structure of S1 (Rayment et al. 1993a, 1993b). The junction between the 25 kDa and 50 kDa domains is known as loop 1 and is located near the nucleotide-binding site. The junction between the 50 kDa to 20 kDa domains is referred to as loop 2 and is situated near the actin-binding site. A narrow cleft separates the upper and lower regions of the 50 kDa domain. Both nucleotide and filament binding sites are positioned on opposite surfaces within the upper and lower regions (respectively) of the 50 kDa domain. Intramolecular communication is therefore required in order for the energy of nucleotide hydrolysis to be used for actin filament translocation. In addition to ATP and actin binding sites, the catalytic domain of S1 is comprised of a core containing a 7-stranded beta sheet, 6 alpha-helices, and several short nucleotide-binding sequences that show tertiary structural resemblance to many other nucleotidases, including GTP-binding proteins, kinesins and the mitochondrial F1-ATP synthase (Goldman 1998). An adjacent "converter domain" links the catalytic core to the 9 nm long alpha helix of the lever arm (neck region) enveloped by calmodulin-like light chains. A battery of biochemical, biophysical and structural methods have shown the converter and lever arm domains rotate relative to the catalytic core in a nucleotide-

Reproduced with permission of the copyright owner. Further reproduction prohibited without permission.

dependent manner (Goldman 1998). Thus muscle myosin moves the actin filament by the angular rotation of its long rigid lever arm.

Myosin Motility Models: Swinging Crossbridge Cycle and the Lever Arm Theory

Many of the classical studies of myosin function have utilized skeletal muscle myosin II (S1). The cross-bridge cycle entails the coupling of a series of biochemical and mechanical events. In muscle, a "rigor" complex consisting of actin tightly bound to S1 is formed in the absence of ATP. Binding of ATP dissociates the S1-actin complex, and the ATP is hydrolyzed to ADP and Pi. Bending of the head domain is coupled to ATP hydrolysis and results in a rocking or tilting motion that moves the head so that it will rebind to a new position on the actin filament. The hydrolysis products remain tightly bound to the catalytic core until the redocking of S1 to the actin filament stimulates the release of Pi and induces a second conformational change, which exerts force through the lever arm and causes the myosin to move along the actin filament. Release of the bound ADP restores the complex to "rigor" state. During most of the ATPase cycle, muscle myosin is either bound weakly to an actin filament or detached from it. Therefore muscle myosin II has a low duty ratio and is nonprocessive (Spudich 1994).

Structural studies of myosin in crystal (Cooke 1993) and solution (Corrie et al. 1999), have shown that the angle of the neck domain relative to the motor domain changes, depending on the form of the bound nucleotide, as a result of minute conformational changes in the catalytic core. On the basis of these findings, a lever arm model have been proposed, in which the neck domain act as a lever arm and the movement is caused by the tilting of the neck domain (Spudich 1994). The hypothesis suggests that the displacement (step-size) and velocity of myosin are proportional to the

Reproduced with permission of the copyright owner. Further reproduction prohibited without permission.

length of the neck. Recent studies however, have challenged this conventional model (reviewed by Geeves 2002). Tanaka et al. (2002) reported that myosin V, an unconventional, processive motor, produced large, 35 nm steps regardless of the length of its neck. This conclusion was drawn from measurements made with molecules of truncation mutants possessing one-sixth of their native neck domains. Furthermore, motility studies of myosin VI, the only known class of minus-end directed myosins also revealed independence between step-size and neck length (reviewed by Geeves 2002).

Regulatory mechanisms in myosins

Actin-activated ATPase activity and motility on actin microfilaments are two diagnostic characteristics of myosins. Both these activities require myosin activation through phosphorylation. For some myosins, activation of these ATP-dependent processes requires phosphorylation in the head domain by a specific myosin heavy chain kinase, whereas others may require phosphorylation in a tail domain. The TEDS rule proposal of Bement and Mooseker (1995) predicts that myosins activated by head phosphorylation will have either a threonine (T) or serine (S) located 16 amino acids upstream from the glutamate (D) in the conserved DALAK amino acid sequence. Myosins that are enzymatically active in the absence of phosphorylation in the head region possess either a glutamate (D) or aspartate (E) at position 16 known as the TEDS rule site; these myosins may require phosphorylation in the tail region or on the light chains.

Phylogenetic classification of myosins

Myosin head domain amino acid sequences are highly conserved and comparisons of these sequences have been used to group myosins into several phylogenetic classes

Reproduced with permission of the copyright owner. Further reproduction prohibited without permission.

(Cope et al., 1996; Garces and Gavin, 1998; Sellers, 2000; Berg et al., 2001). The most comprehensive and up-to-date phylogenetic tree of myosin classes can be accessed from the Myosin Home Page at http://www.mrc-lmb.cam.ac.uk/myosin/myosin.html. The tree in Fig. 1 was reproduced from the Myosin Home Page and is based on the analysis described by Cope et al (1996). Bar diagrams depicting the domain structure of 17 myosin classes are shown in Fig 2. In addition to the well-characterized conventional, two-headed myosin-II of muscle and nonmuscle cells, at least 17 additional classes of myosins have been established, providing evidence of a large and ubiquitously expressed protein superfamily.

Identification of Myo1p in *Tetrahymena*

Although it is generally believed that most eukaryotic cells possess at least one isoform of actin and myosin, existence of these proteins in ciliates was questioned until Cupples and Pearlman (1986) cloned and sequenced actin in the ciliate protozoan *Tetrahymena thermophila.* The presence of actin in *Tetrahymena* invariably led to the speculation about the existence of myosin, and in the decade following the identification of actin, Garces et al. (1998) reported the first ciliate myosin, *MYO1*, in *Tetrahymena thermophila.* In the Garces et al. study, degenerate primers for two regions of sequence homology in the myosin head domain were used in a polymerase chain reaction (PCR) screen of *T. thermophila* genomic DNA to amplify a 765 bp PCR fragment that was cloned and sequenced. Based on the presence of conserved, myosin-specific sequences, the 765 bp PCR product was definitively identified as a fragment of a myosin gene. *MYO1* and its encoded protein Myo1p, were the names given to the newly discovered myosin gene and gene product, according to the rules of nomenclature established at the

Reproduced with permission of the copyright owner. Further reproduction prohibited without permission.

1996 FASEB Ciliate Molecular Biology Meeting. An inverse polymerase chain reaction strategy was used to obtain additional sequence data that included almost the entire head domain of *MYO1*. Alignment of the predicted amino acid sequence of the *MYO1* head domain with known myosins identified the ATP-binding site, a phosphorylation site, and other myosin-specific consensus regions. In a northern blot analysis, a *MYO1*-specific probe detected a 6.6 kb transcript under highly stringent hybridization conditions. Although 2719 bp of *MYO1* genomic sequence was reported by this study neither the N-terminus nor C-terminus was identified. Phylogenetic analysis revealed that the predicted protein encoded by *MYO1* is not a member of any of the previously defined myosin classes and therefore represents a presumptive new myosin class.

EXPERIMENTAL OBJECTIVES

The primary objective of this dissertation is to investigate the cellular function(s) of Myo1p in *Tetrahymena thermophila*. The identification of actin (Cupples et al. 1986) and *MYO1* (Garces et al. 1998) led us to hypothesize that *MYO1*, may affect known actin-related processes in *Tetrahymena*. To test this hypothesis, we employed multiple investigative approaches. Firstly, this study sought to provide insights into putative Myo1p function by through a bioinformatics-based, structural characterization of the protein. Using multiple screenings of genomic and cDNA libraries, in addition to a *MYO1*-based screen of the *Tetrahymena thermophila* genome database, we attempted to determine the complete sequence of *MYO1*, including the identification of its termini.

Secondly, this study used a reverse-genetics approach to investigate Myo1p function. Targeted gene-disruption of the motor domain of *MYO1* was employed to abolish *MYO1* expression in *Tetrahymena*. Phenotypic analysis of the *MYO1*-knockout

Reproduced with permission of the copyright owner. Further reproduction prohibited without permission.

strains was performed in order to assess possible roles of Myolp in cellular processes. This study also interrogated actin-based functions in *Tetrahymena* through perturbation studies, immunolocalization analysis, in vivo tagging with GFP and comparative phenotypic studies between wild type and transformed strains.

Reproduced with permission of the copyright owner. Further reproduction prohibited without permission.

CHAPTER 2

MATERIALS AND METHODS

Creation of the disruption construct

Recombinant DNA protocols described by Sambrook, Fritsch, and Maniatis (1989) were used to create the disruption construct by inserting a *neo* cassette into the coding region of *MYO1*. The cassette (provided by Dr. Martin Gorovsky) consists of a promoter, an antibiotic resistance gene (neomycin), and a terminator sequence cloned into the replicative plasmid pH4T2. Two coding regions flanking the cassette, 1.2 kb and 1.5 kb respectively, were selected from the *MYO1* sequence (Garces and Gavin 1998) and amplified from *Tetrahymena thermophila* genomic DNA by PCR. Downstream and upstream primers contained restriction sites that facilitated subcloning. The gel-purified PCR products were each separately cloned into vector pCR 2.1 (Invitrogen, Carlsbad, CA). Two subcloning steps were required to ligate the 1.2 kb and 1.5 kb regions in flanking positions relative to the cassette as shown in Fig. 7a. Sequencing of the construct confirmed the insertion of the cassette relative to the *MYO1* coding regions.

Somatic transformation of *Tetrahymena*

MYO1 gene knockout. Tetrahymena thermophila strain CU428 was grown to a density of 2.6×10^5 cells/ml in SPP medium (1% proteose peptone, 0.1% yeast extract, 0.2% dextrose, 0.003% sequestrine) and subsequently starved overnight in 10 mM Tris HCl buffer (pH 7.5). Forty ml of starved cells (1×10^7 cells) were centrifuged at 500 *g* for 90 sec and resuspended in 1 ml of the same Tris buffer. The concentrated cells were spread on moist filter paper in preparation for bombardment. Preparation of gold

Reproduced with permission of the copyright owner. Further reproduction prohibited without permission.

particles followed the Large Batch DNA Coating Method (Cassidy-Hanley et al. 1997). Twenty five microliters of a 1.0 micron gold particle suspension (60 mg/ml) were coated with 3 μl of DNA at approximately 2 μg/μl. Cells were bombarded with the DNA-coated gold particles at 900 psi using the Du Pont Biolistic PDS-1000 He particle delivery system (Bio-Rad, Richmond, CA). The biolistic bombardment was performed in the laboratory of Dr. Martin Gorovsky. After bombardment, the cells were immediately resuspended in 50 ml SPP (1×), incubated at 30 °C for 1-2 h, and then plated in 96-well microtiter plates. Two to six hours post-bombardment, 120 μg/ml paromomycin were added to the cells. Three days after the initial antibiotic treatment, cells were screened at 30 °C for transformants. To favor the selection of transformants with complete homozygousity for the disrupted allele, the transformed cells were "walked up" in paromomycin concentration every 24 h in the following sequence: 280 μg/ml, 560 μg/ml, 700 μg/ml, 800 μg/ml, 900 μg/ml, and 1 mg/ml. Transformed cells were grown in 1 mg/ml paromomycin for 600 generations prior to analysis for phenotypic changes. Thereafter, for all experiments cells were grown without paromomycin in a medium containing 2% Bacto-peptone (Difco, Detroit, MI) and 0.4% Bacto-yeast extract (Difco). Periodically, test cultures were grown in the peptone-based medium containing 1 mg/ml paromomycin to confirm their continued resistance to the antibiotic.

GFP-actin transformation. The coding region of the *Tetrahymena* actin gene (GenBank accession number M13939) was amplified from *Tetrahymena* genomic DNA by PCR using primers that added 5' XhoI and 3' ApaI sites to the ends of the amplified sequence. The PCR-amplified actin sequence was cloned into the pVGF-1vector (donated by Dr. Douglas Chalker). The pVGF-1 is a ribosomal DNA-based replicative

Reproduced with permission of the copyright owner. Further reproduction prohibited without permission.

vector that contains a modified micronuclear rDNA gene flanked by the pIC 19 Amp^r *E.coli* vector and a GFP-cassette. The cassette contains the GFP gene (S65T), downstream insertion sites for in-frame cloning of the gene of interest, and flanking regulatory elements consisting of the ribosomal protein rpL29 promoter and both the 5' and 3' UTRs. The amplified sequence was cloned and verified by sequencing, which was also used to confirm in frame insertion. The GFP-tagging construct was introduced into the developing macronucleus by electroporation of conjugating *Tetrahymena*. Electroporation of *Tetrahymena* was performed by Dr. Douglas Chalker. The pVGF-1 vector replicates autonomously to a high copy number as an rDNA mini chromosome and confers paromomycin resistance, allowing for the selection of GFP-expressing transformants. The construct is driven by the rpL29 promoter and achieves highest levels of GFP expression during early log phase of growth. Transformants were maintained at 20 °C in Neff's medium. GFP expression was confirmed by Western blotting.

Southern and Northern blot hybridizations

Genomic DNA was isolated using a DNA Extraction kit (Stratagene, La Jolla, CA), digested with BglII, and resolved on 1% agarose gels, and transferred to Nytran (Schleicher & Schuell, St. Louis, MO) membranes using a TurboBlotter (Schleicher & Schuell). A *MYO1*-specific probe directed against the cloned 1.2 kb *MYO1* coding region was generated by random priming (Amersham, Arlington Heights, IL) and labeled with [α-^{32}P] dCTP (New England Nuclear, Boston, MA). A 524-bp *neo*-specific was restricted from the disruption cassette and labeled as described above. Hybridizations were performed at 68 °C for 2 h in 30 ml of QuikHyb (Stratagene) solution containing 1 mg of sonicated salmon sperm DNA (Stratagene). Membranes were subsequently

Reproduced with permission of the copyright owner. Further reproduction prohibited without permission.

washed twice (15 min each) in 2× SSC with 0.1% SDS at room temperature and once in 0.1× SSC with 0.1% SDS for 30 min at 60 °C followed by overnight exposure to Bio-MS Film (Eastman Kodak, Rochester, NY).

Total RNA was isolated form cultures in exponential phase of growth using the RNAeasy kit (Qiagen, Chatsworth, CA). RNA (82 μg) with an A_{260}/A_{280} ratio greater than 1.8 was separated on 1.5% agarose gels containing 2.2 M formaldehyde. The RNA was transferred to Duralon membranes (Stratagene), and hybridization with a 1.2 kb *MYO1*-specific probe was performed as described for the Southern hybridizations.

DAPI staining

Cells in exponential phase of growth at 20 °C, 30 °C or 35 °C were concentrated by gentle centrifugation and processed for DAPI staining as described by Stuart and Cole (2000).

Morphometry

Cytoplasm/Nucleus Ratios. Cytoplasmic and nuclear areas (μm^2) were measured directly from DAPI-stained cells using an Olympus BH-2 microscope equipped with epifluorescence and a 63× 1.4 N.A. oil immersion lens. For the analysis of macronuclear position or macronuclear division stages, at least 200 DAPI-stained cells were counted in each of three separate experiments and the mean percent with the standard of error was recorded for each determination.

Analysis of GFP-actin Tetrahymena strain. For phenotype analysis, a minimum of 200 DAPI- stained cells or cells fixed in 7% formalin were analyzed using the parameters described above. Living cells were observed and photographed using DIC or phase contrast optics.

Reproduced with permission of the copyright owner. Further reproduction prohibited without permission.

Vacuole distribution. Vacuoles were measured directly from randomly chosen electron micrographs. The nearly spherical appearance of endocytic vacuoles in living *Tetrahymena* is lost when cells are fixed for electron microscopy. All measurements were made using the long axis of the flattened vacuole. It is probable that these measurements included vacuoles of disparate cellular origins and therefore were not restricted to food vacuoles. At least 100 vacuoles were measured from randomly selected micrographs of wildtype and knockout cells. The mean percent of vacuoles in each size range was computed along with a ratio of large vacuoles (> 5.0 μm) to small vacuoles (< 5.0 μm). All values were recorded as mean distributions with the standard error.

Confocal microscopy

Confocal microscopy was performed with a Nikon EFD-3 microscope equipped with a Nikon PCM 2000 confocal laser scanning module (Nikon, Inc., Melville, NY). A 60× 1.4 N.A. Nikon Apochromat oil immersion lens was used to capture images. The S65T GFP spectral variant was excited with the 488 nm line of an argon laser, and a standard fluorescein emission filter was used. Living cells were embedded in 1.5% low-melt agarose 60-90 min prior to use in microscopy. Although cells were embedded in agarose, they exhibited undulating movements that frequently placed a portion of the specimen out of focus. Therefore, the number of confocal scans was limited to 3-4 for averaging. For immunofluorescence studies, cells were prepared for confocal microscopy as described by Stuart and Cole (2000). Anti-actin antibody was conjugated to Alexa Fluor 488 using protocols described by the manufacturer (Molecular Probes, Eugene, OR). Images were stored in a Zip disk (Iomega Corp., Roy, UT) and edited in Adobe Photoshop (Adobe Systems Inc., Palo Alto, CA).

Reproduced with permission of the copyright owner. Further reproduction prohibited without permission.

Electron microscopy

Conventional transmission electron microscopy and post-embedment immunogold electron microscopy utilized protocols described by Gavin et al. (2000). For immunogold labeling, anti-actin and anti-GFP antibodies were used with anti-rabbit IgG secondary antibody conjugated to 10 nm colloidal gold (Nanoprobes, Yaphank, NY). For controls, primary antibody was omitted from the immunolabeling protocol.

Growth curves

Cultures were grown in either a peptone-based medium (described under the *Somatic transformation* sub-section) or Neff's medium (Orias et al. 2000). To achieve a high surface area to volume ratio that ensured optimal oxygenation of the medium, 100 ml of culture medium were used in a 2.8 Fernbach flask. The flask was incubated at constant temperature without shaking. For rapid determinations of cell density, absorbance at 600 nm was measured. For cell number determinations, direct counts of cells were done microscopically.

Latex bead uptake

To assay the rate of phagocytosis, a 10-µl aliquot of Texas Red-conjugated, 2.16 µm-diam. latex beads (Sigma, St. Louis, MO) was added to a 25 ml *Tetrahymena* culture in exponential phase of growth and maintained at the desired temperature for 15 min without shaking. Cells were fixed in a solution of 3.7% formaldehyde, counterstained with DiOC6 (Sigma), and observed with fluorescence microscopy. At least 100 cells were counted in each of three separate experiments for each wildtype and Δ *MYO1* sample. The mean and standard error of beads per cell were recorded.

Reproduced with permission of the copyright owner. Further reproduction prohibited without permission.

For confocal microscopy, a 2 µl of 1.0 µm TransFluoSpheres (Molecular Probes) suspension was added to a 25 ml *Tetrahymena* culture at log phase, maintained at 30 °C for 30 min, and then fixed for immunofluorescence. TransFluoSpheres were excited with the 488 nm line of an argon laser and emitted fluorescence at 644 nm.

Cytochalasin treatment

A 10 mg/ml stock solution of cytochalasin D (CD) with dimethylsulphoxide (DMSO) solvent (Sigma) was used at a final concentration of 40 µg/ml CD and 0.4% DMSO for all experiments. This concentration of the drug has been previously shown to inhibit food vacuole formation (Nilsson 1977). CD was added to 5 ml cell cultures in exponential phase of growth. Control cultures lacked CD but contained 0.4% DMSO. Untreated controls were also used. All cultures were maintained at either 20 °C or 35 °C and monitored for cell growth, food vacuole formation, and macronuclear division over a 24 h period. To monitor food vacuole formation, 2 µl of latex bead suspension were added directly to the cell culture and processed as described in the *Latex bead uptake* sub-section. For DAPI staining, 200 µl aliquots of the cell culture were removed and dried directly onto the surface of a glass slide.

Anti-actin antibody

Polyclonal antibodies were generated against a C-terminus peptide in *Tetrahymena* actin. Antigen injections were performed by Alpha Diagnostic (San Antonio, TX). Rabbit immunoglobin was purified from antiserum by protein A affinity. A 1.0-ml aliquot of Protein A-conjugated agarose beads (Sigma) was briefly equilibrated in 1M Tris pH 7.4 and gently washed by repeated low speed centrifugation until the supernatant showed zero absorbance at 280 nm. A 0.5 ml vol. of antiserum from

Reproduced with permission of the copyright owner. Further reproduction prohibited without permission.

immunized was incubated with the washed beads at 4 °C for 1 h. The beads were gently washed by repeated low speed centrifugation in phosphate-buffered saline (PBS): 137 mM NaCl, 2.7 mM KCl, 10 mM Na_2HPO_4, 1 mM KH_2PO_4 pH 7.0. For elution of IgG, beads were incubated in 1.0 ml of 100 mM glycine pH 3.0 at 4 °C for 10 min. The mixture was centrifuged and the supernatant immediately adjusted to pH 8 by addition of 1.0 M Tris pH 8.0 and dialyzed against PBS.

Electrophoresis and immunoblotting

Lysates were prepared from log phase cultures grown in Neff's medium at 24 °C. Cells were concentrated by centrifugation and resuspended in 100 mM Tris (pH 8.0). A protease inhibitor cocktail as described by Turkewitz et al. (2000) was added to the cell suspension followed by the immediate addition of hot (95 °C) SDS-PAGE sample buffer. The lysis mixture was put through a vortex, incubated at 95 °C for 5 min and immediately incubated on ice for 30 min. Immediately following the incubation on ice, lysis mixtures were centrifuged to sediment insoluble material. Polypeptides were separated on a 4%-12% SDS-PAGE gel and electrophoretically transferred to a PVDF membrane using standard methanol-based transfer protocols. Standard immunoblotting protocols were used for chemiluminescent immunodetection of antigens. Tropix CDP-Star chemiluminescent detection system was purchased from Applied BioSystems (Foster City, CA), mouse anti-GFP antibody from Zymed (San Francisco, CA), alkaline phosphatase-conjugated goat anti-rabbit IgG from Applied BioSystems, and alkaline phosphatase-conjugated goat anti-mouse IgG from Sigma.

Quantitative analysis of immunogold labeling

Reproduced with permission of the copyright owner. Further reproduction prohibited without permission.

Colloidal gold labeling was quantitated by morphometric principles described by Weibel et al. (1966) and used in previous studies by Garces et al. (1995) and Hoey and Gavin (1992). Gold particle densities were computed from random micrographs in at least three labeling experiments. For this study, post-embedment labeling was used, and each electron microscope grid constituted a separate labeling experiment.

Creation and screening of genomic library

To create the library, 0.4 μg of dephosphorylated *Tetrahymena* genomic DNA was cloned into 1.0 μg of the Lambda DASH II vector (Stratagene, La Jolla, CA) and packaged into Gigapack III Gold packaging extracts (Stratagene) using protocols described by the manufacturer. Ligation and packaging efficiencies were assessed using manufacturer-provided controls. The library was titered, plated, and plaque lifts were performed as described by the Lambda DASH II vector kit manual.

A 1.2 kb *MYO1*-specific probe generated by random priming was used to conduct primary, secondary and tertiary hybridization screens according to the probe-labeling and hybridization protocols described in the *Southern and Northern hybridizations* sub-section of the Materials and Methods. Positive recombinant clones were identified and selectively enriched using standard methodology (Sambrook et al.), and DNA isolates were prepared by using a Lambda DNA Isolation Kit from Qiagen. Restriction analysis of recombinant clones was performed by digestion with either BamH I or Not I restriction endonuclease.

cDNA library screening

A plasmid-based *Tetrahymena thermophila* cDNA library, donated by Dr. Aaron Turkewitz, was screened using a one-sided PCR strategy. The library was cloned into the

Reproduced with permission of the copyright owner. Further reproduction prohibited without permission.

plasmid vector pBluscript SK II (Stratagene) and stocks were maintained at a concentration of 175 ng/µl. Amplified stocks of the library were created and maintained at 500 ng/µl concentration. For all PCR screenings, a 100-ng aliquot of library DNA was used per reaction mixture. For one-sided PCR, combinations of vector-specific and *MYO1*-specific primers were used in attempts to amplify *MYO1* cDNA. To test cDNA representation and library integrity, conventional PCR amplifications of actin and a selected 597 bp region of *MYO1* were performed using forward and reverse gene-specific primers.

Polymerase Chain Reaction (PCR) and RT-PCR

All PCR amplifications from genomic or cDNA, were performed using the Advantage 2 Polymerase System (Clontech). Template and primer concentrations, buffer conditions and cycling parameters followed recommended manufacturer protocols. For RT-PCR, total RNA was isolated from log-phase cultures of *Tetrahymena* using TRIzol Reagent (Invitrogen). Messenger RNA was reverse-transcribed using PowerScript Reverse Transcriptase (Clontech) and primed by either an oligo dT_{18} or a *MYO1*-specific reverse primer. Second strand cDNA synthesis followed the standard methodology outlined by Sambrook et al. (1989). All PCR products were TA-cloned into the plasmid vector pCR 2.1 (Invitrogen).

Database Searches

The *Tetrahymena thermophila* Genome Sequencing Project is currently conducted by The Institute for Genomic Research (TIGR) using a whole genome shotgun approach.

Reproduced with permission of the copyright owner. Further reproduction prohibited without permission.

A searchable database derived from the preliminary sequences of the cloned genomic fragments was available on the Institute's web site: www.tigr.org. A Basic Local Alignment Search Tool (BLAST) server facilitated the retrieval of gene-specific sequences from the preliminary contigs.

Reproduced with permission of the copyright owner. Further reproduction prohibited without permission.

CHAPTER 3

DETERMINATION OF THE COMPLETE SEQUENCE OF *MYO1*

CLONING STRATEGIES

Understanding gene function often necessitates a structural characterization of both the gene and its encoded product. A PCR-based strategy was used to identify 2719 base pairs of genomic *MYO1* sequence but neither the 5' nor 3' terminus of the gene was identified. Further, northern blot analysis identified a single *MYO1* isoform 6.6 kb in size, implying that over half of *MYO1* sequence remained undetermined. To determine the complete sequence of *MYO1,* this study employed multiple screenings of genomic and cDNA libraries, in addition to a shotgun genome database search. A lambda-based genomic library was created and screened by hybridization, while a one-sided PCR strategy was used to amplify clones from the plasmid cDNA library.

RESULTS AND DISCUSSION

Genomic library screening by hybridization. A genomic library was created by cloning BamH I-digested genomic DNA purified from *T. thermophila* into the bacteriophage lambda replacement vector, Lambda DASH II. Ideally, to ensure with a 99% probability that all regions of a eukaryotic genome with a complexity of 3×10^9 bp are represented at least once in a library, Poisson statistics dictate that the library should contain at least 10^6 random clones (Davis et al. 1994). This calculation assumes that each clone has a genomic insert 15 to 20 kb in size and that all regions of the genome are incorporated into clones at equal frequency. *T. thermophila* has genomic complexity of 2.2×10^8 bp and under lab conditions we only able to generate titers ranging from 1×10^5

Reproduced with permission of the copyright owner. Further reproduction prohibited without permission.

to 6×10^5 plaque-forming-units (pfu). Given its relative size (an order of magnitude less than titers generated by control DNA), the created library might be best considered a partial complement rather than one containing a full representation of all parts of the *Tetrahymena* genome.

A hybridization screen using a radiolabeled, 1.2-kb *MYO1*-specifc probe identified five positive clones that were selectively enriched by secondary and tertiary screens. DNA isolated from the recombinants, however, was considerably problematic for essential downstream applications such as restriction analysis, subcloning, PCR and sequencing. Some isolates exhibited a transient resistance to cleavage by restriction endonucleases. Repeated propagation of the clones and isolation of the DNA produced yields that retained sensitivity to restriction cleavage and permitted excision of the insert DNA. Restriction analysis (Fig. 3a) showed each clone contained a 14-16 kb insert in addition to the left and right vector arms (21 kb and 9 kb respectively). Attempts to subclone, sequence, or amplify the recombinant DNA by PCR proved unsuccessful. The exact cause(s) of the problems arising from the clone DNA is unknown, although factors such as phage growth conditions, the presence of inhibitory contaminants, and the method of DNA isolation may affect DNA utility.

cDNA library screening by PCR. A *T. thermophila* cDNA library cloned into pBluescript II SK was screened using combinations of vector-specific and *MYO1*-specific primers. To test the library for *MYO1* cDNA representation, a selected 597 bp region of *MYO1* was amplified from the library (Fig. 3b) using a pair of gene-specific primers (Table 1). The sequence derived from the 597 bp PCR product showed almost complete homology to the published genomic sequence of *MYO1* (Fig. 3c). The sequence identity

Reproduced with permission of the copyright owner. Further reproduction prohibited without permission.

of the PCR product confirmed *MYO1* cDNA representation in the library and also established the correct reading frame for the conceptual translation of *MYO1* genomic sequence.

Using the one-sided PCR strategy, however, we were unable to amplify and identify further cDNA sequences upstream or downstream of the 597-bp product. Several combinations of vector-specific and *MYO1*-specific primers (Table 1) gave multiple amplification products clustered closely together when resolved by agarose gel electrophoresis (data not shown). By conducting single primer PCR controls, it was determined that most of the multiple amplification products were generated by single pBluescript-specific primers. These amplifications persisted under a variety of buffering and cycling conditions and made the identification of prospective gene-specific products extremely difficult. The occurrence of vector-generated PCR products may be due to the presence of self-ligated complexes of vector DNA in the library that can probably provide multiple priming sites for the pBluescript-specific oligonucleotides.

Genome database screening for MYO1. At the time of this study, The Institute for Genomic Research (TIGR), initiated the *Tetrahymena thermophila* Genome Sequencing Project, and created a searchable database of preliminary contigs derived from cloned shotgun fragments of the whole genome. The *T. thermophila* genome database was accessed via TIGR's website at www.tigr.org. Using a Basic Local Alignment Search Tool (BLAST) server, multiple matches of high scoring segment pairs (HSPs) with *MYO1* were obtained. From these multiple alignments, the highest scoring preliminary contigs that overlapped with the 5' and 3' boundaries of the partial *MYO1* sequence were identified (Fig. 4). These genomic fragments showed high sequence

Reproduced with permission of the copyright owner. Further reproduction prohibited without permission.

identity to *MYO1* (> 90 %) and were used in a secondary BLAST search to obtain additional 5' and 3'-overlapping contigs. Using this strategy of successive BLAST searches of matching genomic fragments, we were able to assemble 1226 bp of sequence data upstream, and 4351 bp downstream of the published partial *MYO1* genomic sequence (Fig. 4). The total assembled genomic sequence data including the 2719 bp of known *MYO1*, equaled 8298 base pairs.

In order to show that the preliminary contigs were *MYO1*-related based on their positional contiguity, PCR analysis was performed. Primers encompassing selected regions that overlapped known *MYO1* and assembled downstream contigs (Fig. 5a), amplified PCR products whose sizes (1 kb and 2 kb) exactly matched sequence-based predictions (Fig. 5b). Further, PCR was used to amplify a 6.7 kb region (Fig. 5c) based on candidate start and stop sequences that approximated the size of the transcribed *MYO1* gene (6.6 kb).

Once contiguity had been established between the assembled genomic fragments and the partial genomic sequence of *MYO1*, an NCBI-Open Reading Frame (ORF) Finder analysis was conducted to identify candidate reading frames for conceptual translation. Multiple reading frames (+1, +2 and +3) were established for a 7 kb-genomic region and their relative positions are depicted in fig. 6a. Myosin-specific consensus sequences of the *MYO1* head domain were identified within the first two overlapping ORF regions (+1: 1-2682 and +3: 2484-3893) shown in fig. 6a. Gaps and regions of overlap between consecutive ORFs are the prospective intron sites. The aforementioned overlapping ORFs were resolved into a single, uninterrupted 4 kb-translated region after the removal of a putative intron at nucleotide position 2431 to position 2477 (data not shown). This

Reproduced with permission of the copyright owner. Further reproduction prohibited without permission.

intron was first reported by Garces et al. (1998) and was identified using splice boundary consensus sequences (5' GT/3' AG) and AT content. Based on the gaps and overlaps identified from the ORF analysis, at least five introns are hypothesized to exist in the *MYO1* gene. Two putative stop sites were also identified at nucleotide positions 6678 and 7008 that corresponded to different reading frames; +1 and +2 respectively. This disparity between terminator sites can be readily resolved by subsequent sequence comparisons with cDNA data.

Conceptual translation of MYO1. Sequence data compiled from the ORF Finder analysis was then used to conduct a NCBI-BLASTP and Conserved Domain Database (CDD) searches. Translated sequence of Myo1p revealed a primary structure comprising of approximately 2000 amino acids. The predicted domain structure of Myo1p is diagrammatically represented in Fig. 6b. The CDD search revealed the presence of a ~ 750-aa conserved motor domain with almost 100% identity with aligned myosin-specific consensus sequences of the head domain. Interestingly, the motor domain is preceded by a 300-aa region which produced no significant alignments with known proteins. This suggests that Myo1p may possess a unique N-terminal extension in its head domain. Immediately following the motor, a CDD alignment identified two IQ motifs totaling 24 residues. Therefore, we predict that the Myo1p heavy chain is associated with two calmodulin or calmodulin-like light chains.

Beyond the neck, the CDD search established the presence of a Band 4.1, Ezrin, Radixin, Moesin (FERM) domain within the tail region of Myo1p. Also known as talin homology domains, FERM domains are generally believed to mediate structural interactions between the cytoskeleton and the membrane and are hypothesized to bind

Reproduced with permission of the copyright owner. Further reproduction prohibited without permission.

integral membrane proteins (Berg et al. 2000). Three classes of myosins: VII, X and XV, and the divergent myoG in *Dictyostelium* (Titus 2003) are known to possess talin homology domains. Following the 190 aa-FERM domain, Myo1p contains 250-320 aa region (depending on the TGA position) of unique C-term sequence. This property differs from the class VII, X, XV and myoG myosins where the FERM domain occupies the carboxyl terminal end of the protein.

MYO1-cDNA generation by RT-PCR. In order to definitively identify intron/ exon sites and the true termini of *MYO1*, cDNA data was required for comparative analyses with the genomic sequence. A 3.2 kb RT-PCR product was amplified from total *T. thermophila* RNA (Fig. 6c) using a forward primer in the *MYO1*-neck region and a reverse oligomer corresponding to the terminator sequence ending at nucleotide position 7008 (TGA 2). A similar-sized product was generated by PCR from genomic DNA (Fig. 6c) using the same primers. This initial evidence suggests that the terminator codon at position 7008 may be the true stop codon for *MYO1*, however up to the time of this report, the cDNA product remained to be cloned and sequenced. Further, attempts are currently being undertaken to generate cDNA sequences upstream of the 3.2 kb product.

Reproduced with permission of the copyright owner. Further reproduction prohibited without permission.

CHAPTER 4

A GENOMIC KNOCKOUT OF *MYO1*

EXPERIMENTAL DESIGN

The identification of *MYO1* in *Tetrahymena* provided us with an opportunity to employ a reverse-genetics approach to investigate gene function. Significant progress has been made in the development of methods for the manipulation of the *T. thermophila* genome, including high frequency transformation, gene replacement and gene knockout technologies. Targeted disruption of *MYO1* was achieved by the insertion of a neomycin (*neo*) gene into the coding region of the *MYO1* motor domain. A disruption construct was delivered to the macronucleus by biolistic bombardment and was targeted to the *MYO1* locus by homologous recombination.

RESULTS AND DISCUSSION

Genetic Characterization of Transformants

A MYO1 construct transformed Tetrahymena. Transformants were selected for resistance to paromomycin and subsequently used for phenotypic analysis. To confirm that the transformation was both stable and complete, transformants that had been grown continuously for ~600 generations in 1 mg/ml paromomycin were subsequently grown in the absence of the drug for ~600 generations and then returned to 1 mg/ml paromomycin-treated medium without loss of cell density. Southern hybridization analysis showed that paromomycin-resistant cells contained the cassette within the *MYO1* gene. A 1.2 kb *MYO1*-specific probe hybridized to a single 14 kb fragment of Bgl II-digested genomic DNA from wild-type cells (Fig. 7b). The same probe hybridized to slightly larger 15.5

Reproduced with permission of the copyright owner. Further reproduction prohibited without permission.

kb fragment of Bgl II- digested genomic DNA from transformed (Δ) *MYO1* cells but it did not hybridize to a 14 kb fragment, an indication that the 1.4 kb cassette had been inserted into the *MYO1* coding region (Fig. 7b). A *neo*-specific probe hybridized to the 15.5 kb genomic fragment from Δ *MYO1*; it did not hybridize to wild-type DNA (Fig. 7c).

PCR amplification of DNA from transformed cells further confirmed the existence of the construct and the disruption of the wild-type allele. *MYO1*-specific primers were used to amplify genomic DNA from both wild-type and transformant cells. In wild-type DNA the upstream and downstream primers are separated by only 0.1 kb. However, in transformed DNA these primers are separated by an additional 1.4 kb due to insertion of the cassette. PCR amplification of wild-type DNA produced a single component at 0.1 kb, whereas amplification of transformed DNA yielded a 1.5 kb product (Fig. 7d). The 0.1 kb product was not observed in PCR amplifications of transformed DNA. Northern blot hybridization was used to determine whether *MYO1* transcription was disrupted by insertion of the cassette. The *MYO1*-specific probe that was used for the Southern blot hybridization was also used in a northern blot analysis of both Δ *MYO1* RNA and wild-type RNA (Fig. 7e). The *MYO1*-specific probe hybridized to a 6.6 kb RNA from wild-type; it did not hybridize to RNA from Δ *MYO1*.

Phenotypic Analysis

Transformed MYO1 cells have a smaller cytoplasm/nucleus ratio than wild-type. Cytoplasm/nucleus (Cyt/Nu) ratios were computed for both wild-type and Δ *MYO1* at 20 °C and at 35 °C (Fig. 8). At 20 °C the mean (Cyt/Nu) ratio was 16.2 ± 3.9 for wild-type and 11.7 ± 5.2 for Δ *MYO1*, $p < 0$. At 35 °C the mean ratio was 11.4 ± 4.0 for wild-

Reproduced with permission of the copyright owner. Further reproduction prohibited without permission.

type and 7.8 ± 2.9 for Δ *MYO1*, $p < 0$. Wild-type cells grown in the presence of cytochalasin D did not have an altered Cyt/Nu ratio.

Doubling time for populations of Δ MYO1 cells is conditionally higher than wild-type. Growth rates of transformed and wild-type cells were evaluated in mass cultures maintained at constant temperature without shaking. At 35 °C populations of Δ *MYO1* and wild-type had similar doubling times of approximately 7 h. However, at temperatures lower than 35 °C, doubling times of the two populations were markedly different. At 20 °C, the average doubling time for the Δ *MYO1* population was ~23 h during exponential growth phase, in contrast to the 14-h doubling time for wild-type populations. At 20 °C Δ *MYO1* reached saturation density in about 80 h in contrast to 200 h for wild-type, and the saturation density for wild-type were significantly higher than the saturation density for Δ *MYO1*. Saturation densities at 35 °C were comparable in the two strains.

In wild-type cultures grown in the presence of CD, cytokinesis appeared normal, although cell doubling times were 1.8 times longer than for DMSO-treated controls. The saturation density of wild-type populations cultured in the presence of CD reached the same level as in DMSO-treated controls. However, the time required to reach saturation density in the presence of CD was greater than that for DMSO-treated controls. Our findings on the effects of CD are in close agreement with those previously reported by Nilsson (1977).

Transformed MYO1 cells have a reduced rate of food vacuole formation at 20 °C. At 20 °C, wild-type cells accumulated beads three times faster than Δ *MYO1* cells, whereas bead uptake at 35 °C was similar in both wild-type and Δ *MYO1* (Table 2).

Reproduced with permission of the copyright owner. Further reproduction prohibited without permission.

Wild-type cells grown in the presence of CD displayed a similar reduction of food vacuole formation. The rate of food vacuole formation in CD-treated wild-type cells was ~1.5% of the rate observed for DMSO-treated controls (Table 2).

Macronuclear division in wild-type Tetrahymena. Analysis of DAPI-stained cells was used to establish a series of continuous stages in the macronuclear division process (Fig. 9). The macronucleus was centrally located in most cells. Prior to the onset on macronuclear elongation, the macronucleus is known to migrate anteriorly and then posteriorly (Nilsson 1999). In this study, phase contrast and DIC microscopy were used to confirm the anterior to posterior migration of the macronucleus. Elongation of the macronucleus began while the macronucleus was located in the posterior region of the cell (Fig. 9, Stage I). Elongation continued until the distended nuclear material spanned almost the entire length of the two prospective post-division cells (Fig. 10a). The fully elongated macronucleus constricted at its midpoint, which coincided with the fission line (Fig. 9, Stage III; Fig. 10a). At the constriction site, the fully elongated macronucleus separated into two subnuclei resulting in the segregation of the G2 macronucleus to the two post-division cells (Fig. 9, Stage IV; Fig. 10b). Thin strands of nuclear material between the two separating nuclei were frequently released during macronuclear division (Fig. 10b). Separation of the constricted macronucleus was completed prior to the completion of cytokinesis (Fig. 10b). The entire process of macronuclear division in wild-type *Tetrahymena* was the same at either 20 °C or 35 °C in the presence or absence of CD.

Transformed MYO1 cells have a defect in macronuclear elongation. Although micronuclear division and cytokinesis appeared normal in Δ *MYO1* cells, conspicuous

Reproduced with permission of the copyright owner. Further reproduction prohibited without permission.

defects in macronuclear elongation were observed in cells grown at either 20 °C or 35 °C. In the majority of cells in populations of exponentially growing Δ *MYO1*, the macronucleus was located at one end of the cell (Table 3). In some of these cells, the stage 0 macronucleus failed to elongate and remained nearly spherical in the posterior region of the cell, although cytokinesis was subsequently achieved (Fig. 10c-f; Fig. 11). In other Δ *MYO1* cells, macronuclear elongation was initiated. However, elongation proceeded more slowly than in wild-type cells as indicated by the higher percentage of macronuclear stage I in Δ *MYO1* cultures (Table 4). Macronuclear elongation in these cells was frequently inhibited, although cytokinesis was completed (Fig. 10c-f, Fig. 11). Failure of Δ *MYO1* cells to initiate or complete macronuclear elongation resulted in post-division cells that contained either the entire G2 macronucleus from the previous cell cycle (Fig. 10e, 10f), more than half of the G2 macronucleus (Fig. 10d), less than half of the G2 (Fig. 10d), or none of the G2 macronucleus (Fig. 10e, 10f). Morphometric analysis (Fig.8) showed that at 20 °C approximately 30% of a Δ *MYO1* population had abnormally low cytoplasm/nucleus ratios, an indication that grossly unequal segregation of the macronucleus had occurred.

MYO1 affects the endocytic pathway and population doubling time. In *Tetrahymena*, the endocytic cycle involves multiple events including membrane transport, fusion and recycling in the food vacuole-forming region of the oral structure. A food vacuole originates from several precursor vesicles that fuse with the plasma membrane in the oral region and eventually separate from it (Rasmussen 1976). The nascent vacuole then fuses with lysosome membranes to form a mature food vacuole (Kitajima and Thompson 1977; Rasmussen 1976). Although actin has been localized to

Reproduced with permission of the copyright owner. Further reproduction prohibited without permission.

the food vacuole-forming region of the *Tetrahymena* oral apparatus (Méténier 1984), the precise involvement of actin in this process remains obscure. In this study, the treatment of cells with cytochalasin and the ablation of *MYO1* expression both resulted in inhibition of food vacuole formation, an indication that Myo1p-actin interaction is required for endocytosis in *Tetrahymena*. The effect of *MYO1* on food vacuole formation was more pronounced at 20 °C than at 35 °C. This temperature dependence probably reflects functional redundancy that compensates for the loss of Myo1p. At the restrictive temperature, the putative redundant motor or redundancy mechanism might not be fully operative, and the loss of Myo1p becomes more acute for the cell.

The reduced rate of food vacuole formation at 20 °C is a probable contributing factor to the increased doubling time observed at that temperature. At 35 °C, population doubling times for wild-type and transformants were nearly the same, even though many cells in the Δ *MYO1* population had aberrant macronuclear division. Cells with too much macronuclear DNA could have an accelerated generation time, whereas cells with low macronuclear DNA content will have an abnormally long generation time. However, doubling time reflects both the fast-dividing cells and the slow ones within a population. In a population of Δ *MYO1*, the fast-dividing cells presumably increased the average doubling time of the population so that it approximates the doubling time of the wild-type population.

Myolp-macronuclear interactions with sub cortical actin could determine macronuclear elongation. Data presented in this study suggest that Myo1p contributes to macronuclear elongation. Transformed *MYO1* cells frequently failed to either initiate or complete macronuclear elongation, and consequently, macronuclear segregation was

Reproduced with permission of the copyright owner. Further reproduction prohibited without permission.

grossly unequal. Morphometry confirmed the existence of cells with abnormally large macronuclei and abnormally small Cyt/Nu ratios. The larger than wild-type mean size of macronuclei is consistent with grossly unequal macronuclear segregation as a consequence of aberrant macronuclear elongation. However, other factors unrelated to macronuclear division could also affect nuclear size in Δ *MYO1* cells. The morphometric analysis also indicated that division progeny with abnormally high macronuclear DNA content are viable. *Tetrahymena* is known to regulate DNA content by altering both the timing and the extent of DNA synthesis. If DNA content is too low, cells go through an additional synthesis prior to G2 (Worthington et al. 1976), and if DNA content is too high, an S period will be followed by two consecutive cell divisions (Doerder and DeBault 1978). Release of chromatin extrusion bodies may also regulate DNA content (Clefmann 1980).

The underlying basis for macronuclear elongation is not known. Intramacronuclear actin has been reported (Hirono et al. 1987), although the role of this actin in macronuclear division is undetermined. Macronuclear elongation could be achieved, in part, by the motor function of Myo1p in association with a cytoplasmic array of actin microfilaments. Myo1p could also organize the putative cytoplasmic actin array, and perturbation of this cytoskeletal structure through the loss of *MYO1* expression could result in aberrant macronuclear elongation. However, in this study, defects in macronuclear division were not detected in cytochalasin-treated wild-type *Tetrahymena*. Correct macronuclear elongation may require microtubules in cooperation with actin microfilaments. Intranuclear microtubules exist in the *Tetrahymena* macronucleus, although they are not organized into a spindle apparatus and do not appear to be essential

Reproduced with permission of the copyright owner. Further reproduction prohibited without permission.

for macronuclear separation (Jaeckel-Williams 1978). However, in the presence of the microtubule antagonist colchicine, *T. thermophila* cells frequently displayed unequal segregation of the macronucleus during division (Jaeckel-Williams 1978). A more recent study (Fujiu 2000), described an elaborate system of microtubules assembled inside the macronucleus and between the macronucleus and the cortex. During macronuclear division, intramacronuclear microtubules were reported to undergo multiple organizational changes: from a random pattern prior to division, to a radial and subsequently, a parallel organization during elongation (Fujiu 2000). Macronuclear division may therefore be the functional outcome of microfilament-microtubule-based synergistic processes.

Analysis of a *Tetrahymena* strain lacking a functional *MYO1* gene revealed multiple effects on cell structure and function, notably food vacuole formation (endocytosis) and macronuclear division. Evidence presented in this study suggests that the molecular basis of both processes requires the participation of Myolp-actin-based contractile systems.

Reproduced with permission of the copyright owner. Further reproduction prohibited without permission.

CHAPTER 5

EXPRESSION OF GFP-ACTIN IN *TETRAHYMENA*

EXPERIMENTAL DESIGN

Although the actin cytoskeleton is a ubiquitous feature of eukaryotes, there is considerable diversity in its organization within various cell types. In ciliates, sub-plasma membrane differentiations define a region known as the cortex, which contains basal bodies, accessory microtubules, actin microfilaments and other types of filamentous structures. The ciliate cortex possesses the fibrillar architecture that would be described as the cytoskeleton in other cell types. Ciliate actins are known to be divergent from other actins. For example, *Tetrahymena* actin is only 75% homologous to yeast actin (Cupples and Pearlman 1986), and this divergence is associated with some unusual and interesting properties. *Tetrahymena* actin does not bind phalloidin (Hirono et al. 1989), and although cytochalasin has an effect on various functions in *Tetrahymena*, the dosage of the drug required to elicit an effect is typically far above the level required for other eukaryotes (Zackroff and Hufnagel 1998).

There are relatively few studies that have focused on actin localization in *Tetrahymena*. Actin has been localized to a filamentous cage surrounding both somatic and oral region basal bodies (Hoey and Gavin 1992), the food vacuole forming region of the oral structure (Metenier 1984), the contractile ring (Hirono et al. 1987) and the macronucleus (Hirono et al. 1987). The investigation of myosin function invariably raises questions concerning the possible role(s) of actin in *MYO1*-affected processes in *Tetrahymena*. Previous studies of actin antagonists in *Tetrahymena* (Nilsson 1977;

Reproduced with permission of the copyright owner. Further reproduction prohibited without permission.

Zackroff and Hufnagel 2002) and cytochalasin-based perturbation experiments discussed in the previous chapter, all show inhibition of food vacuole formation. Δ *MYO1* strains also exhibited slower rates of food vacuole formation and these observations collectively suggest that *MYO1* may function in concert with its contractile partner, actin, in the endocytic pathway. To investigate further the distribution and function of actin in *Tetrahymena*, a *T. thermophila* strain that expresses GFP-actin in addition to endogenous actin was developed by Conjugal Electroporation Transformation (CET) of a recombinant rDNA-based vector, pVGF-1. The results of this study are summarized and discussed in the section below.

RESULTS AND DISCUSSION

GFP-Actin Expression

Anti-actin antibody. Polyclonal antibodies were raised against a C-terminus peptide of *Tetrahymena* actin. Antibody specificity was evaluated by immunoblotting (Fig. 12). The antibodies detected a single band at 42 kDa, which is the predicted molecular mass of *Tetrahymena* actin based on the sequence reported by Cupples and Pearlman (1986). As a control for antigen specificity, the antibodies were immunoreactive to rabbit muscle actin (data not shown).

A transformed Tetrahymena strain expresses GFP-actin. A strain that expresses GFP-actin was developed by transforming *Tetrahymena* with pVGF-1, an rDNA-based replicative/expression vector. In order to demonstrate expression of GFP-actin in the transformed strain, immunoblots containing total protein were separately probed with anti-GFP and anti-actin peptide antibodies. An anti-GFP antibody detected a 72-kDa protein on immunoblots of total protein from transformed cells (Fig. 12). The 72-kDa

Reproduced with permission of the copyright owner. Further reproduction prohibited without permission.

band was commensurate with the predicted size of the GFP-actin fusion protein and was not detected in wild-type lysates. (Fig. 12). The anti-actin peptide antibody detected *Tetrahymena* actin and the 72-kDa GFP-actin fusion protein on immunoblots of total protein from transformed cells. (Fig. 12). The anti-actin antibody also detected an additional polypeptide (~ 50 kDa), which is a presumed degradation product of the GFP-actin fusion protein (Fig. 12). This degradation product of GFP-actin apparently did not contain an epitope that could be detected by the monoclonal GFP antibody and was not observed on immunoblots probed with anti-GFP antibody. Levels of GFP-actin expression were qualitatively assessed by comparing fluorescent intensity of cells cultured at 20 °C and 30 °C. Fluorescence of transformed cells was more intense at 30 °C than at 20 °C. The temperature-dependent effect on levels of GFP-actin was consistent with construct expression under the influence of the ribosomal protein promoter rpL29.

GFP-actin localizes to known sites of actin. Previous studies have shown that actin in *Tetrahymena* is localized to basal bodies (Gonda et al. 1999; Hirono et al. 1987; Hoey and Gavin 1992) and the contractile ring (Gonda et al. 1999; Hirono et al. 1987). In this study, confocal microscopy of living *Tetrahymena* expressing GFP-actin revealed a fluorescence pattern consistent with basal body localization of the fusion protein. Three different confocal images, each in a different focal plane through the cortex of the same living cell, showed loose punctate fluorescence in longitudinal arrays (Fig. 13 upper panel). Living, wild-type cells displayed autofluorescence as shown in three confocal images of the same cell (Fig. 13). Autofluorescence bleached much more rapidly than GFP-fluorescence (data not shown). Confocal microscopy of living, transformed cells

Reproduced with permission of the copyright owner. Further reproduction prohibited without permission.

revealed a ring of GFP-actin that appeared to be the cytokinesis-related contractile ring in dividing cells (Figs. 13 lower panel). The unusual shape of the dividing cell in Fig. 13 is due to undulating movements while embedded in agarose.

Immunogold electron microscopy confirmed GFP-actin localization to basal bodies. Basal bodies in *Tetrahymena* and other ciliates are surrounded by fibrillar attachments that form a cage (Hoey and Gavin 1992; Williams 1986). In *Tetrahymena*, filaments at the distal and proximal ends of the basal body cylinder form, respectively, the top and base of the cage. The cage walls consist of filamentous partitions that connect to basal body triplet microtubules through a network of thin filaments. Cage structure is more elaborate in the oral apparatus than in kineties. An ultrastructural study showed that anti-actin antibodies localized to fibrillar material forming the walls, base, and top of basal body cages (Hoey and Gavin 1992). In the present study, immunogold localization utilized the anti-GFP antibody that detected GFP-actin on the immunoblot shown in Fig. 12. The anti-GFP antibody labeled components of the basal body cage complex in cells expressing GFP-actin (Fig. 14a-e). In Fig. 14a-c, the three, dense, vertically oriented structures in each figure are fibrillar partitions that form cage walls between adjacent basal bodies, which are not in the plane of section. The cage walls are labeled with small clusters of colloidal gold particles (arrowheads) at the proximal and distal ends. In Fig. 14c, colloidal gold particles (arrowheads) decorate the proximal region (cage base) of one basal body and the distal region (cage top) of another basal body. The image in Fig. 14e shows colloidal gold labeling of somatic basal bodies near the oral cavity in a cell expressing GFP-actin. In order to show that the anti-GFP localization was consistent with an earlier study of actin localization (Hoey and Gavin

Reproduced with permission of the copyright owner. Further reproduction prohibited without permission.

1992), the anti-actin peptide antibody was used in the immunogold labeling technique with wild-type cells. The anti-actin peptide antibody labeled basal bodies and fibrillar material associated with basal bodies (Fig. 14d). Only randomly dispersed colloidal gold labeling was observed with secondary antibody controls (data not shown). Morphometry was used to quantitate colloidal gold labeling. Mean relative particle densities and standard errors are reported in Table 5. Wild-type cells labeled with anti-actin antibody and GFP-actin transformant cells labeled with anti-GFP antibody showed similar relative particle enrichments significantly above background (Table 5).

Phenotypic Analysis

GFP-actin transformants exhibit failure of both macronuclear elongation and cytokinesis. Permanent stock cultures of GFP-actin transformants were maintained at 20 °C. For phenotypic analysis, temporary 30 °C-stock cultures were established and maintained for two days with daily subculturing prior to use in an experiment. At 30 °C, doubling times for the strain expressing GFP-actin and the wild type strain were 18 h and 8 h, respectively. At 20 °C, the average doubling time for the strain expressing GFP-actin was ~26 h, in contrast to the 14-h doubling time for wild type populations.

Macronuclear division was monitored in cultures of the GFP-transformant strain and in a wild-type control. For phenotype analysis, a minimum of 200 DAPI-stained cells or cells fixed in 7% formalin were counted in each of three separate experiments, and the mean percent for each determination was recorded with the standard error. After 12 h growth at 30 °C, macronuclear elongation had failed to occur in 25% of a population of GFP transformants even though micronuclear division had been completed and a division furrow had been initiated (Table 6, Fig. 15a, 15b). In that same population 6%

Reproduced with permission of the copyright owner. Further reproduction prohibited without permission.

displayed apparently normal macronuclear elongation. At 20 °C macronuclear elongation had failed to occur in only 2% of the population (Table 6). Failure of macronuclear elongation coincided with arrest in cytokinesis (Fig. 15a, 15b). The percentage of arrested cells in the population was strongly dependent on the culture temperature. Populations grown at 30 °C contained 10x more arrested cells than populations grown at 20 °C (Table 6). Most arrested cells became homopolar doublets with two sets of oral structures (Fig. 15c, Table 6). Homopolar doublets are known to arise from cells arrested in cell division (Frankel 1989). The single macronucleus and the two micronuclei in an arrested cell (Fig. 15a) became the nuclei for the doublet phenotype (Fig. 15b). After 36 h at 30 °C more than 70% of the population consisted of the doublet phenotype (data not shown). Doublets did not appear to complete division. Cell number declined rapidly with prolonged culture at 30 °C.

Macronuclear elongation and cytokinesis are dependent on both actin and myosin. Phenotypic analysis of the genomic knockout of *MYO1*, indicated that macronuclear elongation and cytokinesis are likely to occur through separate mechanisms that are dependent upon both actin and myosin (Garcés and Gavin 1998). Approximately 25% of transformed *MYO1* cells failed to either initiate or complete macronuclear elongation, although cytokinesis in these cells was often unaffected. In the present study, failure of macronuclear elongation and cytokinesis is a likely consequence of incorporation of GFP-actin into the proposed actin/myosin systems. GFP-actin expression is under the control of the ribosomal protein promoter (rpL29) and is most active during the early phase of logarithmic growth. Therefore, one would expect expression levels of GFP-actin to increase during periods of rapid cell proliferation, e.g.,

Reproduced with permission of the copyright owner. Further reproduction prohibited without permission.

at 30 °C. Consistent with this interpretation is the observation that failure rates for macronuclear elongation and cytokinesis were drastically higher at 30 °C than at 20 °C.

A macronuclear elongation system might involve actin filaments, microtubules, and appropriate motor proteins. It is noted that there was no apparent localization of GFP-actin to the macronucleus. Actin and other components of the elongation machinery could be transiently associated with the nucleus either directly on the nuclear membrane or in the surrounding cytosol through an actin microfilament scaffold. The present study demonstrates that perturbation of the actin component in the elongation machinery can disrupt macronuclear elongation. GFP-actin is almost twice the size of endogenous actin, and whenever the ratio of GFP-actin to endogenous actin is high, e.g., at 30 °C, incorporation of significant amounts of GFP-actin into the elongation machinery could impair its function. Alternatively, the relatively large size of GFP-actin could prevent its incorporation into an elongation system, and the consequent deficiency in actin content would impair nuclear elongation. Although this study suggests that impairment of actin-based function is related to the relative size and quantity of the GFP-actin fusion protein, ratios of GFP-actin to endogenous actin were not definitively quantitated. The precise nature of GFP-actin dysfunction in Tetrahymena can be further explored with quantitative assessments of fusion-protein expression, in vitro studies of f-actin and f-GFP-actin assembly, and filament binding/sliding assays.

As noted above, genomic knockout of *MYO1* disrupted macronuclear elongation, an indication that a myosin is a component of the nuclear elongation machinery. The precise role of myosin in macronuclear elongation has not been clearly established. One possibility is that *MYO1* organizes actin filaments that are involved in nuclear elongation.

Reproduced with permission of the copyright owner. Further reproduction prohibited without permission.

However, *Tetrahymena* is known to have at least four other unconventional myosins (Someya et al. 2000), any one of which could be part of a redundant system for nuclear elongation. Formation of an actin contractile ring prior to the onset of cytokinesis is well documented in *Tetrahymena* (Numata and Gonda 2001). In the present study, contractile rings that may have incorporated a high ratio of GFP-actin to endogenous actin apparently did not properly constrict the cytoplasm, and consequently, cytokinesis was disrupted.

GFP-actin correctly localizes to known actin-containing structures in *Tetrahymena*. However, incorporation of GFP-actin may lead to arrest in macronuclear elongation and cytokinesis, an indication that actin is required for both processes. Although GFP-actin can interfere with the apparent functioning of actin-containing structures, the GFP-actin transformant strain can be used to monitor actin distribution and dynamics and is therefore an important new tool for further studies of *Tetrahymena* actin. The technique of in vivo GFP-tagging is envisaged ideally to assess distribution and expression dynamics of a given protein of interest. In using this approach, there is an implicit assumption that fusion with GFP does not alter the native function of the tagged protein. Based on the evidence reported by the present study, this is not always the case. In addition, a vector-based expression of GFP-actin in *Dictyostelium* resulted in a dominant negative effect of the fusion protein, inhibiting cytokinesis, cell locomotion, and drastically altering cell morphology (Aizawa et al. 1997). The dynamics of GFP-actin in *Tetrahymena* can perhaps be further enhanced if ectopic expression is under the control of an inducible promoter, a technique recently developed in this model system.

Reproduced with permission of the copyright owner. Further reproduction prohibited without permission.

CHAPTER 6

IMMUNOLOGICAL AND ULTRASTRUCTURAL EVIDENCE FOR THE ROLES OF ACTIN AND MYO1P IN THE ENDOCYTIC PATHWAY

EXPERIMENTAL DESIGN

Internalization of fluids or particulate matter at the cell surface is an essential cellular process. Studies of several model systems have demonstrated that endocytic pathways involve specific membrane receptors, actin-dependent redistribution of the plasma membrane, membrane fusion to engulf fluids and/or particulates, maturation of nascent endocytic vacuoles, and signaling pathways that regulate the entire process (Engquvist-Goldstein and Durbin 2003; May and Machesky 2001; Maniak 2002, 2003; Qualmann et al. 2000; Soldati 2003; Sorkin 2000). Although actin is generally thought to be removed from the vacuole prior to vacuole maturation, mature phagosomes and other endocytic vacuoles interact with the actin cytoskeleton and have actin-based motility (Taunton et al. 2000; Zhang et al. 2002). Myosins from several classes are involved in various phases of the endocytic pathway (Soldati 2003; Titus 2000a,b; Tuxworth and Titus 2000). In *Dictyostelium*, Myo I-A, Myo I-B, and Myo I-C are involved in fluid phase pinocytosis (Neuhaus and Soldati, 2000; Novak et al. 1995), and Myo I-B is involved in the recycling of endosomal components into the plasma membrane (Neuhaus and Soldati 2000). Class I myosins *MYO3* and *MYO5* are required for polarization of the actin cytoskeleton and for fluid phase endocytosis in *Saccharomyces* (Goodson et al. 1996).

Reproduced with permission of the copyright owner. Further reproduction prohibited without permission.

In *Tetrahymena* and in other free-living ciliates, the highly differentiated oral cavity (oral apparatus) is a major pathway for plasma membrane internalization. Membrane internalization originates from several precursor vesicles is known as a nascent food vacuole (early endosome/phagosome). The major steps in the endocytic pathway are depicted in Fig. 16. Nascent food vacuoles are rapidly expanded through a series of several vacuole-vacuole fusions (vacuolar expansion). Expanded vacuoles become acidified by subsequent fusion with lysosomes (acidification/maturation) followed by the final endocytic phase of egestion of vacuolar wastes and recycling of the vacuolar membrane at a specialized membrane region known as the cytoproct (vacuolar recycling).

In *Tetrahymena*, membrane invaginations at sites known as parasomal sacs and located adjacent to somatic basal bodies are probable sites of another pathway for endocytosis, and vacuoles that originate from this pathway have been described as having a coated appearance (Nilsson and van Deurs 1983). Coated pits and coated vesicles have also been reported in *Paramecium.* However, there is no further evidence that connects the coated morphology with clathrin in either organism. In *Tetrahymena*, it is not known whether food vacuole formation is receptor-mediated and/or constitutive and receptor-independent. Relatively few studies have attempted to define biochemical and morphological markers for stages of vacuole maturation in *Tetrahymena*. Earlier studies recognized membrane fusions as integral to the maturation process (Kitajima and Thompson 1977; Rasmussen 1976). Studies of *Tetrahymena* indicate the involvement of microtubules, cytoplasmic dynein, actin, and myosin in endocytic pathways. A *Tetrahymena* cytoplasmic dynein gene knockout phenotype showed inhibition of

Reproduced with permission of the copyright owner. Further reproduction prohibited without permission.

phagocytic activity, an indication that microtubules are involved in the endocytic pathway (Lee et al. 1999). Studies of actin antagonists show that they inhibit food vacuole formation (Nilsson 1977; Zackroff and Hufnagel 2002). A phenotypic analysis of Δ*MYO1* cells (Chapter 4) revealed food vacuoles formed at a slower rate than in wild-type cells. Regulation of food vacuole formation in *Tetrahymena* could involve a feedback loop that coordinates vacuole formation with vacuole maturation. In this study, the basis for the reduced rate of food vacuole formation in the *MYO1*-knockout strain was investigated by comparative analyses of vacuole morphology and actin organization in knockout and wild type cells using transmission electron microscopy and confocal immunofluoresence microscopy.

RESULTS AND DISCUSSION

Actin associates with developing food vacuoles. In *Tetrahymena*, plasma membrane at the base of the buccal cavity is a major site of internalization of fluids and particulates within food vacuoles. Food vacuole formation and maturation were studied by allowing cells to internalize latex beads and subsequently using anti-actin antibody to image these cells with confocal microscopy (Fig. 17). The immunofluorescence images of wild-type (Fig. 17a, 17c) and *MYO1*-knockout (Fig. 17b) cells show localization of actin to oral region and somatic basal bodies consistent with previous studies of actin localization in *Tetrahymena* (Hoey and Gavin, 1992). The bright green ring of fluorescence on the upper left margin of the cell (17a, 17b) is in the oral apparatus. The cell in Fig. 17c is in an early stage of division and has two oral apparatuses but the division furrow has not formed. Enlarged images of the buccal cavity show bead-containing vacuoles positioned internal to the base of the cavity (Fig. 17d, 17e). These

Reproduced with permission of the copyright owner. Further reproduction prohibited without permission.

vacuoles display yellow fluorescence due to the colocalization of the red fluorescent bead and green fluorescence of the immunostained actin. Food vacuoles throughout the cytosol of wild-type and knockout cells contained patches of yellow fluorescence (Fig. 17b, 17c) which coincided with ciliary meridians. Most vacuoles qualitatively did not display as much yellow fluorescence as vacuoles located near the buccal cavity (Fig. 17a, 17b). However, at the posterior end of the cell, vacuoles displayed bright yellow fluorescence (Fig. 17c). Actin immunolocalization patterns for wild-type and *MYO1*-knockout cells were essentially the same (Fig 17a, 17b), and suggests that the presence of Myo1p is not a requirement for the organization of actin microfilaments within the buccal cavity and along the ciliary meridians.

Confocal immunofluorescence microscopy revealed that actin colocalized with nascent vacuoles within the food vacuole-forming region of the buccal cavity. This association of actin with nascent food vacuoles may reflect the role of actin as a cytoskeletal prerequisite for membrane internalization and nascent vacuolar expansion.

Vacuoles in MYO1-knockout cells are smaller than vacuoles in wild type-cells. Conventional transmission electron microscopy (TEM) revealed significant differences in vacuole morphology between wild-type and *MYO1*-knockout cells. Food vacuoles in the *MYO1*-knockout strain were smaller than vacuoles in wild-type cells (Fig. 18). Both wild-type and *MYO1*-knockout strains contained populations of variably-sized vacuoles. Given this heterogeneity in size, vacuoles were grouped and measured into three diameter ranges (Table 7). The ratio of vacuoles > 5.0 μm to vacuoles < 5.0 μm was significantly lower in the *MYO1*-knockout strain than in wild type (Table 7).

Reproduced with permission of the copyright owner. Further reproduction prohibited without permission.

Wild-type and *MYO1*-knockout strains also differed in the patterns of vacuole distribution within cells. *MYO1*-knockout cells exhibited considerable accumulations of nascent vacuoles proximal to the oral region (Fig. 18b, 18c) whereas the equivalent subcellular region in wild type contained larger vacuoles that had already undergone significant expansion (Fig. 18a). Expanded vacuoles are present throughout wild-type cells (Fig. 18d) while *MYO1*-knockouts contained dense accumulations of substantially smaller endosomes (Fig. 18e) and multi-vacuolar aggregates (Fig. 18f). Vacuolar aggregates were comprised of clusters of small vacuoles loosely connected by slender vacuolar extensions (Fig. 18f).

Nascent food vacuoles are generally thought to be rapidly expanded through multiple fusions with other vacuoles. In the absence of *MYO1*, ultrastructural evidence showed that cells accumulate smaller vacuoles which may reflect an inhibition of rapid vacuolar expansion. Defects in vacuole-vacuole expansion is further corroborated by the presence of multi-vacuolar aggregates in *MYO1*-knockout cells; a morphologically distinct product of inhibited vacuolar fusion. TEM analysis of vacuole morphology suggests a role for Myo1p as a translocatory component facilitating rapid vacuole expansion during the early stages of the endocytic pathway.

Reproduced with permission of the copyright owner. Further reproduction prohibited without permission.

CHAPTER 7

CONCLUSIONS, WORK IN PROGRESS AND FUTURE DIRECTIONS

Structural characterization of Myo1p. This study has focused upon determining the cellular functions of Myo1p in the ciliate protozoan *Tetrahymena thermophila.* By screening the *Tetrahymena* genome database, the complete genomic sequence of *MYO1* was determined, permitting a qualified structural characterization of its encoded protein, Myo1p. From the genomic sequence data, *MYO1* is a 7 kb-gene encoding a ~2000 aa-heavy chain polypeptide. The size of the genomic *MYO1* sequence is consistent with the the 6.6 kb transcript identified by northern blot analysis (Garces et al. 1998).

Myo1p is predicted to have a 300 aa-N-terminal extension, a 750 aa-conserved motor domain, two IQ motifs, and a 190 aa-FERM domain located 250-300 residues from the C-terminal end of the protein. The domain architecture of Myo1p presents some unique and interesting features. Six classes of myosins are known to possess N-terminal extensions: classes III, IX, XII, XV, XVI and XVIII (Berg et al. 2001). Most of these extensions are structurally uncharacterized and functionally undetermined. The extended region in class III myosins contains a kinase domain, whereas classes XVI and XVIII possess ankyrin-repeats and PDZ motifs, respectively, within their N-term extensions. The N-terminal extension of the Myo1p head domain produced no significant alignments with known proteins, and may therefore constitute a unique and novel region within the heavy chain polypeptide.

The tail region of Myo1p also revealed unusual features in its domain structure. Myo1p is predicted to contain a single FERM domain 250-300 aa away from the

Reproduced with permission of the copyright owner. Further reproduction prohibited without permission.

carboxyl terminal. FERM domains are membrane-binding domains and are present in proteins (erzin, radixin, moesin, band 4.1, talin) that play structural and regulatory roles in the assembly and stabilization of specialized plasma membrane regions. Although there are three myosin classes (VII, X, XV) and at least one other divergent myosin (myoG) that bear talin homology (FERM) domains, the predicted the tail structure of Myo1p is significantly different. Firstly, the FERM domains in the aforementioned classes are present with other conserved sub-regions within the tail, notably tail homology domains (MyTH4), Src homology 3 (SH3) and pleckstrin homology (PH) domains (Fig. 2). The deduced sequence of Myo1p showed only a single FERM domain present in the tail region. Secondly, in the talin homology myosins, the FERM domain occupies the C-term end of the protein (classes VII and XV each contain two FERM domains with one at the C-terminus and the other further upstream within the tail). The FERM domain identified in Myo1p, in contrast, does not occupy a strict C-term position but is followed by a 250-300 aa stretch of unique sequence. These novel structural features can indeed raise speculations of whether they confer to Myo1p unique properties related to its role in cellular processes.

Myo1p function in macronuclear elongation and vacuolar fusion. The evidence presented in this study suggests that Myo1p, in concert with actin, play key roles in macronuclear division and the endocytic pathway. *MYO1*-knockout cells exhibited defects in macronuclear elongation resulting in unequal macronuclear segregation during division. Phagocytosis was also inhibited in *MYO1*-knockouts and accumulations of abnormally-small, incompletely-fused vacuoles were present in cells in the form of multi-vacuolar aggregates. Furthermore, perturbation of actin dynamics in wild type with

Reproduced with permission of the copyright owner. Further reproduction prohibited without permission.

cytochalasin severely inhibited phagocytosis, while copious expression of GFP-actin in transformed cells recapitulated the aberrant macronuclear phenotype of the *MYO1*-knockout. Based on the structural, morphological and functional analyses conducted, this study proposes a conjectural model of Myo1p function in macronuclear elongation and vacuolar fusion depicted in Fig. 19. In both dynamic processes, Myo1p is proposed to be associated with either the vacuolar membrane or the nuclear envelope via the interaction of its putative FERM domain and integral membrane proteins (Fig. 19c). The motor domain can bind actin microfilaments and Myo1p is hypothesized to power the translocation of the organelle to facilitate macronuclear elongation and rapid vacuolar fusion. The association of actin with nascent vacuoles in the oral region may provide the cytoskeletal architecture necessary for Myo1p-based translocation of vacuoles to each other for rapid expansion through membrane fusion. Significant actin localization in the peri-macronuclear region was not detected, but putative microfilament arrays that can act as tracks for Myo1p-powered macronuclear elongation may be transient in its organization and dependent on the cell's division cycle. The proposed model does not preclude the possibility of a structural role for the Myo1p-actin complex in macronuclear and vacuolar positioning.

Head domain analysis has phylogenetically defined Myo1p as a novel, divergent unconventional myosin (Garces et al. 1998). Unclaimed by any of the established classes and being the first ciliate myosin identified, invariably raised speculations of whether Myo1p is involved in cellular processes particular to ciliates, or more general myosin-associated functions. The results of this study demonstrate that the roles of Myo1p in *Tetrahymena* are related to both speculated aspects of cell function. As discussed in

Reproduced with permission of the copyright owner. Further reproduction prohibited without permission.

chapter 6, classes of myosins are thought to play a variety of roles in the endocytic pathway, including recycling of endosomal components to the plasma membrane, vesicle transport, and fluid-phase pinocytosis. Myolp's role in vacuolar expansion during early endocytosis may belong to a set of general cell functions mediated by unconventional myosins. The amitotic division of the macronucleus, however, is a biological feature unique to ciliates. In most eukaryotic cells nuclear division events are mediated by the microtubule-based mitotic spindle and its associated motors. Myolp function in macronuclear elongation suggests a novel role for myosin involvement in nuclear division.

Future directions. To further the structural characterization of Myo1p, this study is currently attempting to obtain cDNA data using a RT-PCR strategy. A 3.2 kb cDNA product corresponding to the putative tail region of *MYO1* has recently been amplified from total *Tetrahymena* RNA, but remains to be cloned and sequenced. Perhaps the most significant aspect of Myolp function that still remains undetermined is its cellular localization. With the elucidation of the Myo1p sequence, antibodies against the highly variable regions of the tail domain can be generated for immunolocalization studies. Antibodies against the tail domain can also be used to probe for candidate partner proteins via immunoprecipitation and pull-down assays. Alternatively, GFP-tagging of the substrate-specific tail domain can be done to investigate Myo1p's sub-cellular location in vivo. Given *Tetrahymena's* tractable genetic system, we will have the opportunity to create multiple deletion mutants for selected regions of the *MYO1* gene. These deletion mutants can be instructive in assessing domain-specific functions within the protein. Finally, as Myo1p is the founding member of a presumptive new class of

Reproduced with permission of the copyright owner. Further reproduction prohibited without permission.

myosins, the completion of the *Tetrahymena* genome project will afford this study the search for related members of this new myosin class. As many as six myosin genes are reported to exist in *Tetrahymena* (Someya et al. 2000), four of which are believed to be related (based on their partial cDNA sequences) to *MYO1*. Gleaning sequence data of these myosin genes from the genome database will provide the opportunity to establish definitive structural and functional class-specific properties of *Tetrahymena* myosins.

Reproduced with permission of the copyright owner. Further reproduction prohibited without permission.

	PRIMER DESCRIPTION	DIRECTION	SEQUENCE
Disruption construct & probe	1.2 kb *MYO1* coding region w/ Nhe I site (probe)	Forward	5'GCTAGCTTATTCAATCAGTATAAAAA 3'
	1.2 kb *MYO1* coding region w/ Xma I site (probe)	Reverse	5'CCCGGGGTAGTATTTCTTAAGTTTT 3'
	1.5 kb *MYO1* coding region w/ Sal I site	Forward	5'GTCGACTCTGAGTTACTCTAAGTTAA 3'
	1.5 kb *MYO1* coding region w/ Mlu I site	Reverse	5'ACGCGTGTACTCTTTTTCCTTAGGAA 3'
	MYO1 primer flanking neomycin cassette insertion site	Forward	5'AAAGTTAAGCGACACTCAG 3'
	MYO1 primer flanking neomycin insertion site	Reverse	5'AAATACTAAAGACTCTTCAA 3'
GFP-actin construct	Actin (1.2 kb) w/ Xho I site	Forward	5'CTCGAGATGGCTGAAAGTGAA 3'
	Actin (1.2 kb) w/ Apa I site	Reverse	5'GGGCCCGCTTAAAATAAAAT 3'
	GFP-construct sequencing primer	Forward	5'ACCACATGGTCCTTCTTGAG 3'
	GFP-construct sequencing primer	Reverse	5'TTGTATGATATATGAGCATAT 3'
cDNA library	*MYO1*-cDNA primer (597 bp)	Forward	5'TGGACGAGGTAACGGAAA 3'
	MYO1-cDNA primer (597 bp)	Reverse	5' AGTTGGAGCCTGAGTGTCGC 3'
	MYO1-cDNA primer (5' region)	Reverse	5'CATAATTTCCTTTTCTAATAA 3'
	MYO1-cDNA primer (3' region)	Forward	5'AAAACAAAAAGGATTAACATT 3'
MYO1-contigs	*MYO1*-genomic (3'region)	Forward	5'CATAAGAATTTAATGAAAAT 3'
	Genomic contig (1 kb amplification)	Reverse	5'TCTGCATACTAATAAGCAGG 3'
	Genomic contig (2 kb amplification)	Reverse	5'ATATATAAAAAGCGAAGTAA 3'
	Genomic contig (6.7 kb amplification)	Forward	5'ATGATATGTGAGTATATTGA 3'
	Genomic contig (6.7 kb amplification)	Reverse	5'TCATTTAGTGTTTTAATTT 3'
RT-PCR	RT-oligo dT primer	Reverse	$(T)_{18}$
	MYO1@ nt position 7008	Reverse	5'TCATTGACTTTTTTTCTTATT 3'
vector	T3 primer	Forward	5'AATTAACCCTCACTAAAGGG 3'
	T7 primer	Reverse	5'GTAATACGACTCACTATAGGGC 3'

Table 1. List of Primers (restriction site sequences are underlined)

Reproduced with permission of the copyright owner. Further reproduction prohibited without permission.

Strain	°C	Beads Per Cell
wild type	20	3.1 ± 0.05
ΔMYO1	20	1.0 ± 0.1
wild type (CD)	20	0.04 ± 0.01
wild type (DMSO)	20	2.8 ± 0.05
wildtype	35	5.5 ± 0.05
ΔMYO1	35	5.6 ± 0.1
wild type (CD)	35	0.03 ± 0.01

Table 2. Uptake of latex beads by wild type and *ΔMYO1 Tetrahymena thermophila*

Reproduced with permission of the copyright owner. Further reproduction prohibited without permission.

Strain	Temperature	Central	Non-central
Δ *MYO1*	20 °C	26 ± 7.3	74 ± 7.3
Wild type	20 °C	94 ± 1.3	6 ± 1.3
Δ *MYO1*	35 °C	46 ± 8.4	54 ± 8.4
Wild type	35 °C	95 ± 1.0	5 ± 1.0

Table 3. Macronuclear position in exponentially growing wild type and Δ *MYO1* *Tetrahymena thermophila.*

Reproduced with permission of the copyright owner. Further reproduction prohibited without permission.

		Percentage of dividing cells in macronuclear division stage			
Strain	**Temp.**	**I**	**II**	**III**	**IV**
Wild type	20 °C	11 ± 0.5	67 ± 0.8	6 ± 3.1	16 ± 3.8
Δ *MYO1*	20 °C	26 ± 1.9	57 ± 4.5	10 ± 2.7	7 ± 0.3
Wild type	35 °C	12 ± 0.6	58 ± 0.9	10 ± 3.4	20 ± 2.6
Δ *MYO1*	35 °C	18 ± 2.3	66 ± 3.8	12 ± 4.1	14 ± 1.7

Table 4. Distribution of macronuclear division stages in exponentially growing wild-type and Δ *MYO1 Tetrahymena thermophila.*

Reproduced with permission of the copyright owner. Further reproduction prohibited without permission.

		Relative particle density		
Strain	**Antibody**	**Basal bodies**	**Background**	**Total particles**
Wild type	Anti-actin	0.902 ± 0.02	0.098 ± 0.02	912
GFP-actin	Anti-GFP	0.881 ± 0.03	0.119 ± 0.03	353

Table 5. Immunogold localization of actin to basal bodies.

Reproduced with permission of the copyright owner. Further reproduction prohibited without permission.

	Singlet	Normal Dividers	Arrested	Doublet
30 °C	57 ± .08	6 ± .06	25 ± .09	12 ± .27
30 °C	59 ± .02	3 ± .15	4 ± .23	34 ± .08
20 °C	89 ± .03	3 ± .2	2 ± .3	6 ± .19

Table 6. Morphometry of GFP-actin strain of *Tetrahymena thermophila*

Reproduced with permission of the copyright owner. Further reproduction prohibited without permission.

Strain	Percent of Vacuoles			*Ratio
	> 5 μm	1.0 – 5.0 μm	< 1.0 μm	
Wild type	24.5 ±4.4	29.3 ± 1.8	46.2 ± 7.4	0.27 ± 0.07
MYO1 knockout	0.4 ±0.36	39.6 ± 13.7	60.0 ± 14.0	0.005 ± 0.02

Table 7. Morphometry of Vacuole Distribution

Reproduced with permission of the copyright owner. Further reproduction prohibited without permission.

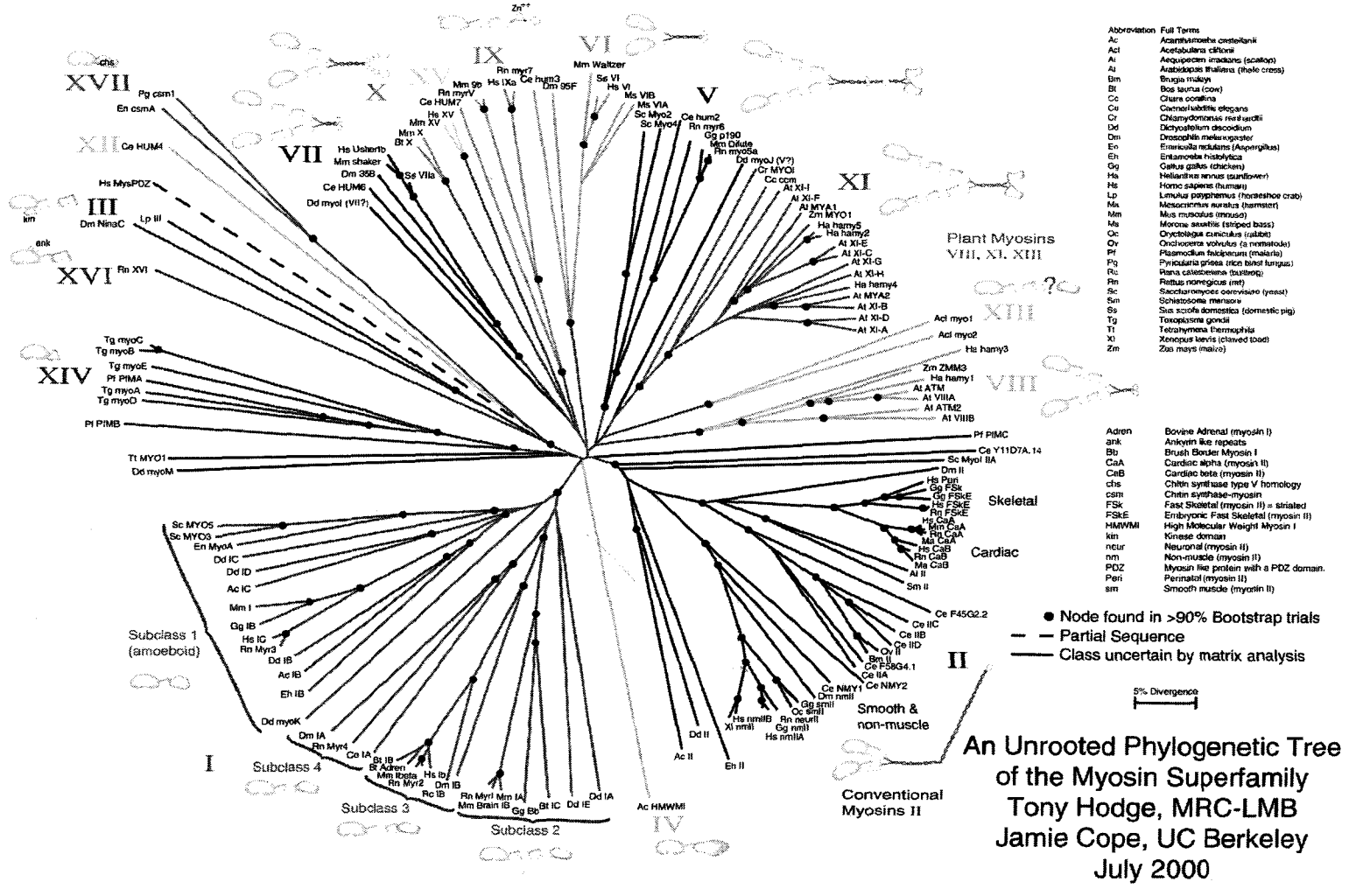

Fig. 1. An Unrooted Phylogenetic Tree of the Myosin Superfamily. This tree was reproduced from the Myosin Homepage (www.mrc-lmb.cam.ac.uk.myosin/myosin.html) according to the website's stipulations.

Reproduced with permission of the copyright owner. Further reproduction prohibited without permission.

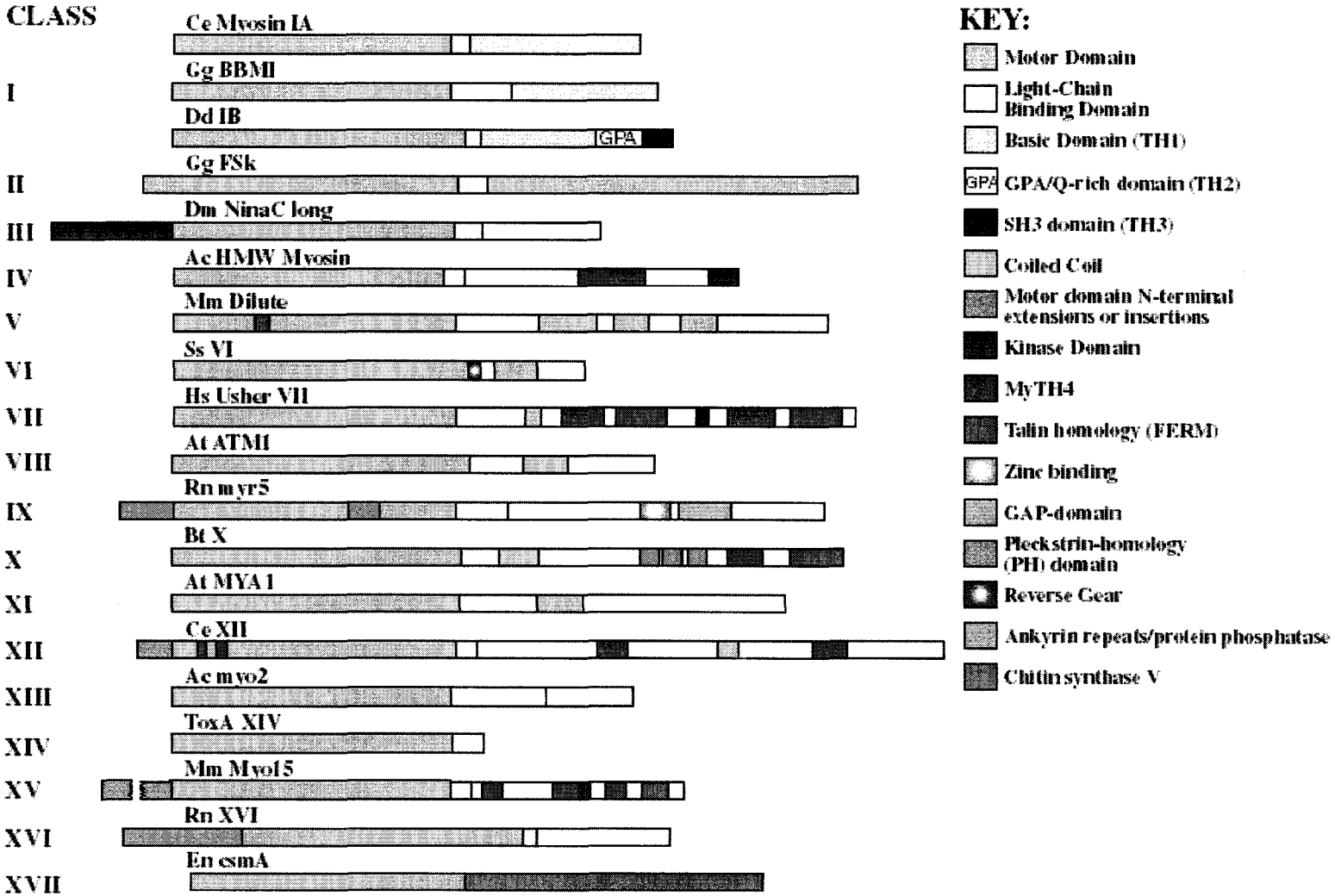

Fig. 2. The Myosin Classes. The bar diagrams were reproduced from the Myosin Homepage according the website's stipulations. For references, see Mooseker and Cheney (1995), and Sellers (2000).

Reproduced with permission of the copyright owner. Further reproduction prohibited without permission.

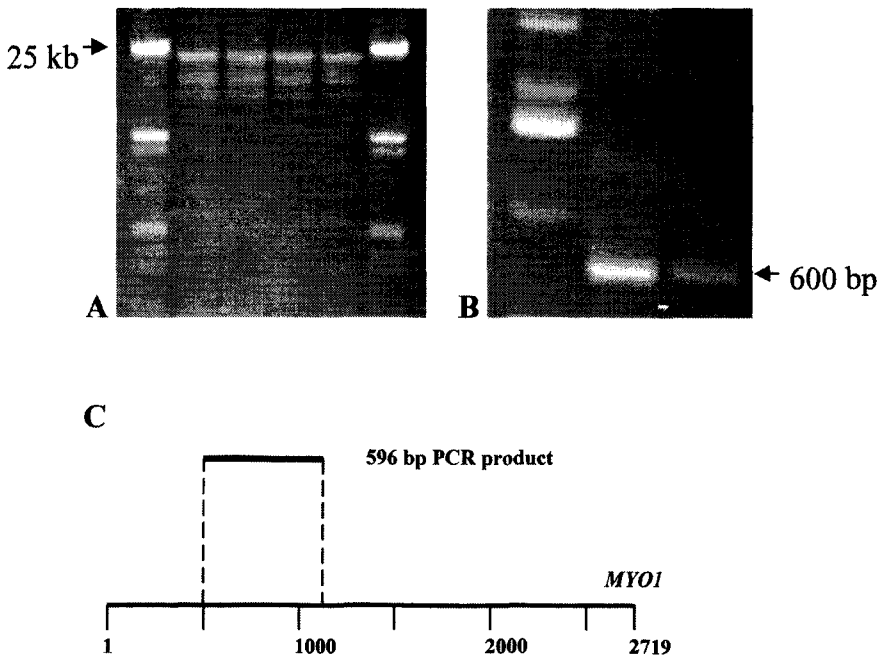

Fig. 3. Genomic clones and cDNA amplification products derived from library screens.

A. BamH I digest of four genomic clones isolated by *MYO1*-probed hybridization screens of a lambda-based *T. thermophila* genomic library. The clones' DNA are flanked by EcoR I- and Hind III-digested lambda DNA markers.The gel profile shows the recombinant DNA resolved into three bands; top band: 21 kb (left vector arm), middle band: ~14 kb (insert), bottom band: 9 kb (right arm). **B.** A 596 bp PCR product amplified from a *T. thermophila* cDNA library using *MYO1*-specific forward and reverse primers. Two identical PCR reactions are shown on this gel; DNA markers are on the left. **C.** Positional alignment of the cDNA PCR product with the genomic sequence of *MYO1*.

Reproduced with permission of the copyright owner. Further reproduction prohibited without permission.

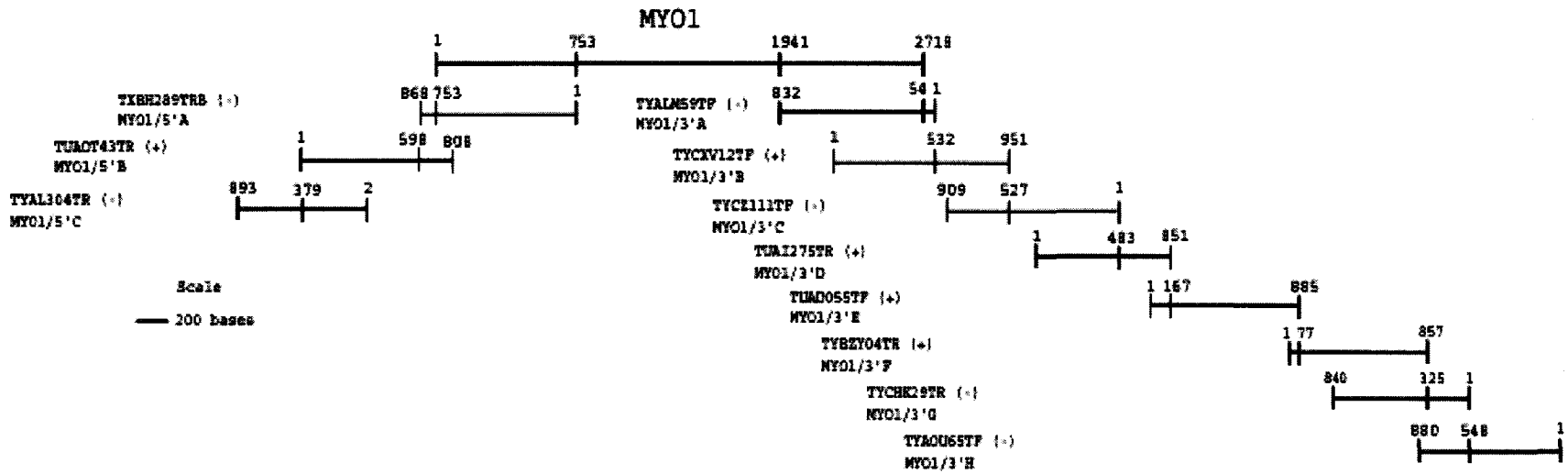

Fig. 4. A map of *MYO1* and aligned preliminary contigs. A BLAST server was used to screen the *Tetrahymena* genome database for match genomic fragments (contigs) that overlapped the 5' and 3' boundaries of *MYO1* (2718 bases). Contigs were assigned two designations: the top name is the TIGR database designation, eg. TYALM59TF (-); the name below is the designation assigned by this study. Each fragment was labeled according to the relative order of their proximity to the 5' or 3' end of *MYO1*, eg. "MYO1/3'A" is the designation given to the first identified contig overlapping the 3' end of *MYO1*.

Reproduced with permission of the copyright owner. Further reproduction prohibited without permission.

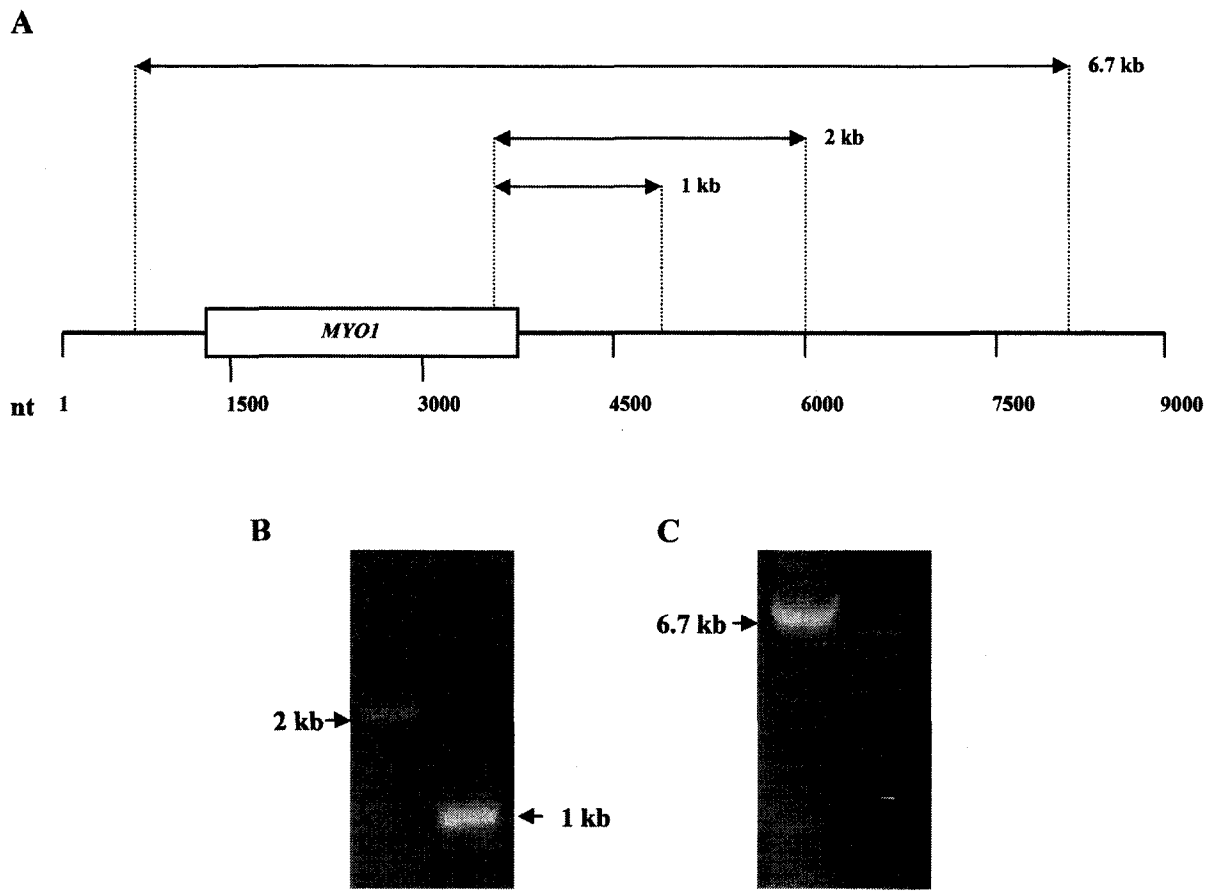

Fig. 5. Verification of *MYO1* genomic contigs by PCR. A. Sequence data obtained from the Tetrahymena genome database was assembled relative to the published partial sequence of *MYO1* (bar). Relative postions of the amplified regions are shown by arrowhead lines. Assembled sequences totaled 8298 base pairs. **B.** To show that the preliminary contigs were contiguous with the published *MYO1* data, selected downstream sequences, 1 kb and 2 kb respectively, were amplified from genomic DNA. The forward primer used for both amplifications was proximal to the 3' boundary of the published *MYO1* partial sequence. **C.** A 6.7 kb PCR product was obtained using primers representing candidate start and stop sequences and corresponding to the approximate size of the *MYO1* gene. DNA markers are shown in the left lane.

Reproduced with permission of the copyright owner. Further reproduction prohibited without permission.

A. Establishment of *MYO1* Open Reading Frames (ORFs)

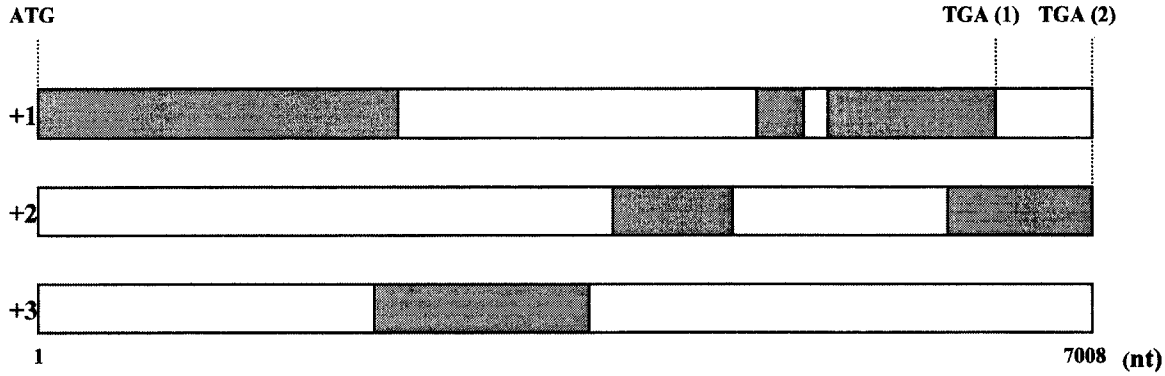

Frame	Nucleotide Position	Length (bp)
+1	1-2682	2682
+3	2484-3893	1410
+2	4502-4951	450
+1	4951-5226	276
+1	5575-6678	1104
+2	6378-7008	612

B. Predicted Domain Structure of Myo1p

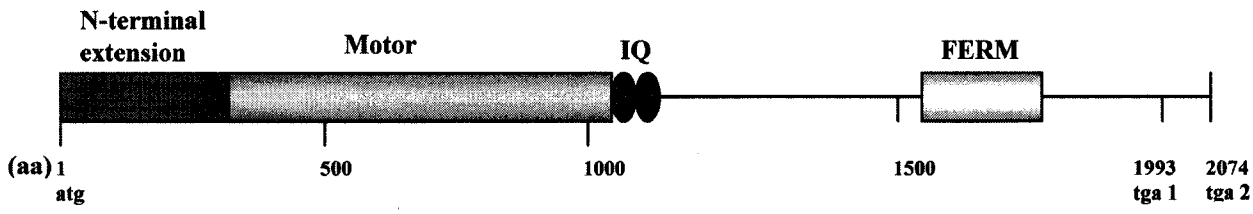

C. RT-PCR analysis of *MYO1*

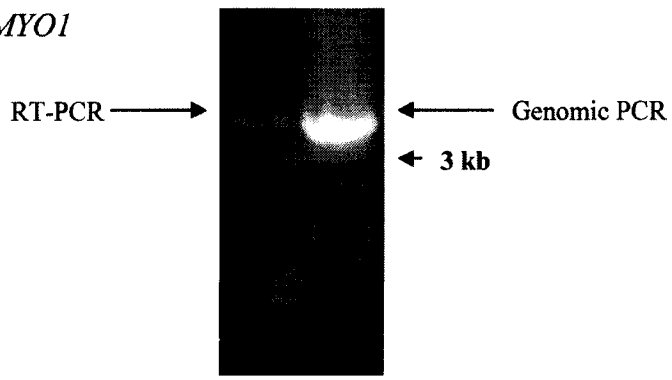

Fig. 6. Open Reading Frames, Domain Structure and RT-PCR of Myo1p. A. ORFs (gray bars) were established from *MYO1* genomic sequence data using a NCBI-ORF Finder analysis. ORFs are listed in relative order from start (ATG) to stop (TGA) codons. Two putative stop codons are shown. **B.** Conceptual translation of Myo1p revealed the presence of an N-terminus extension, the conserved motor domain, two IQ motifs and a FERM domain. **C.** A 3.2 kb RT-PCR product corresponding to the neck and tail regions was obtained from total RNA (left lane). A similar-sized product was amplified from genomic DNA using the same primers (right lane).

Reproduced with permission of the copyright owner. Further reproduction prohibited without permission.

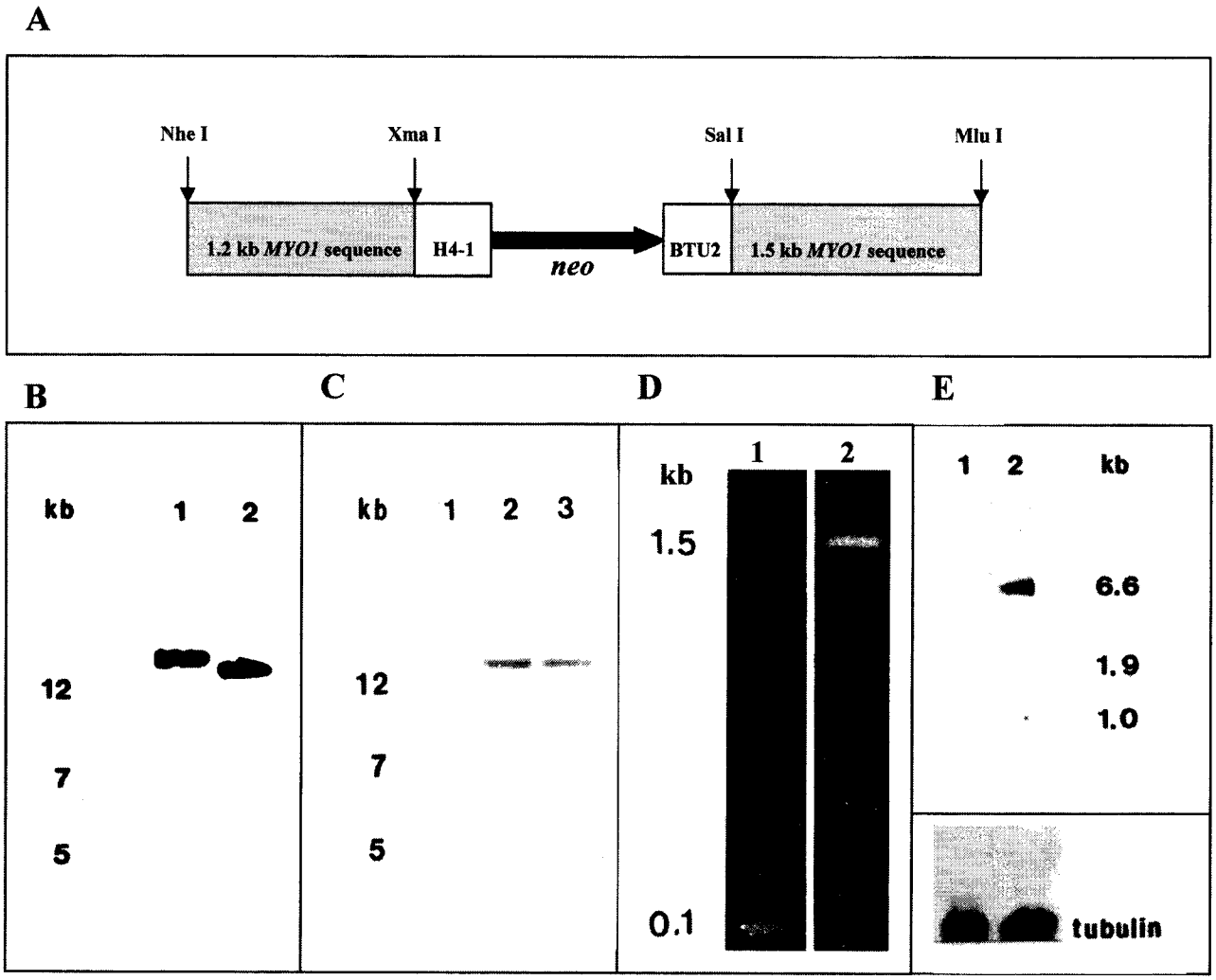

Fig. 7. A *MYO1* construct transformed *Tetrahymena thermophila.*
A. A diagram of the disruption construct. The construct contained a cassette consisting of a promoter (H4-1), an antibiotic resistance gene (neo), and a terminator sequence (BTU2), all flanked by selected *MYO1* coding regions (gray). **B.** Southern blot of genomic DNA probed with a 1.2 kb *MYO1*-specific probe. Lane 1: Δ *MYO1*. Lane 2: Wild-type. The probe hybridized to a single genomic fragment of Bgl II-digested genomic DNA from wild-type cells (Lane 2). The same probe gave a solitary hybridization signal at a slightly larger (15.5 kb) fragment of Bgl II-digested genomic DNA from Δ *MYO1* cells (Lane 1). **C.** Southern blot of genomic DNA probed with a 524 bp *neo*-specific probe. Lane 1: Wild-type. Lanes 2 & 3: Two independently established Δ *MYO1* cell lines. The *neo*-specific probe hybridized to the 15.5 kb genomic fragment from Δ *MYO1*; it did not hybridize to wild-type DNA. **D.** PCR amplification of genomic DNA. Lane 1: Wild-type. Lane 2: Δ *MYO1*. Amplification of wild-type DNA produced a single component at 0.1 kb, whereas amplification of transformed DNA yielded a 1.5 kb product. **E. Upper Panel:** Northern blot of total RNA probed with the 1.2 kb *MYO1*-specific probe. Lane 1: Δ *MYO1*. Lane 2: Wild-type. The probe hybridized to a 6.6 kb RNA from wild-type; it did not hybridize to Δ *MYO1* RNA. **E. Lower Panel:** A tubulin control for gel sample loading.

Reproduced with permission of the copyright owner. Further reproduction prohibited without permission.

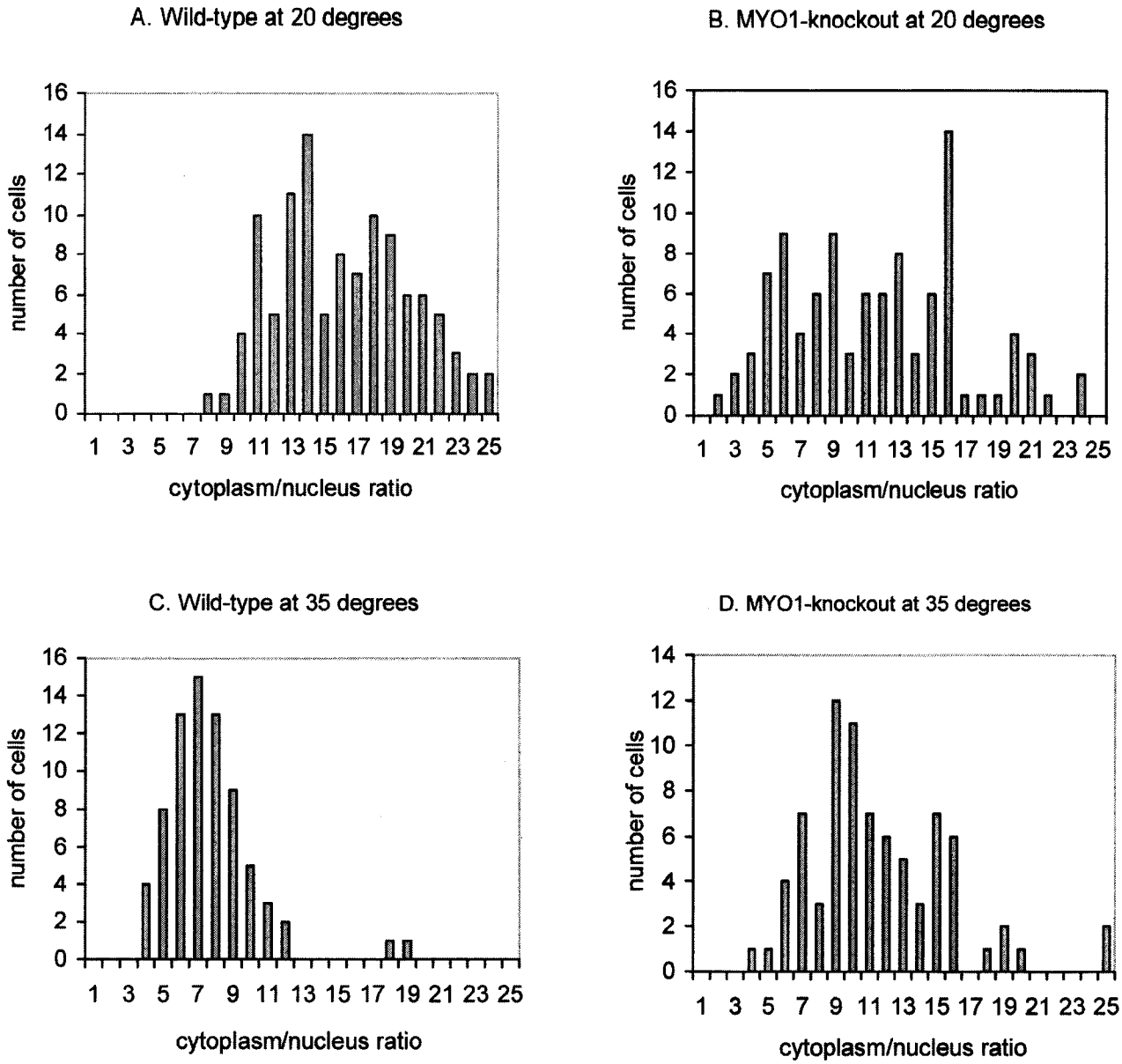

Fig. 8. Morphometry of wild-type and *ΔMYO1* populations of *Tetrahymena thermophila* grown at 20 ^{0}C and at 35 ^{0}C as described in the MATERIALS AND METHODS (chapter 2). After 30 h of growth, each population was processed for DAPI staining. Cytoplasmic and nuclear areas were measured from DAPI-stained cells, and the cytoplasm/nucleus ratio computed for each cell.

Reproduced with permission of the copyright owner. Further reproduction prohibited without permission.

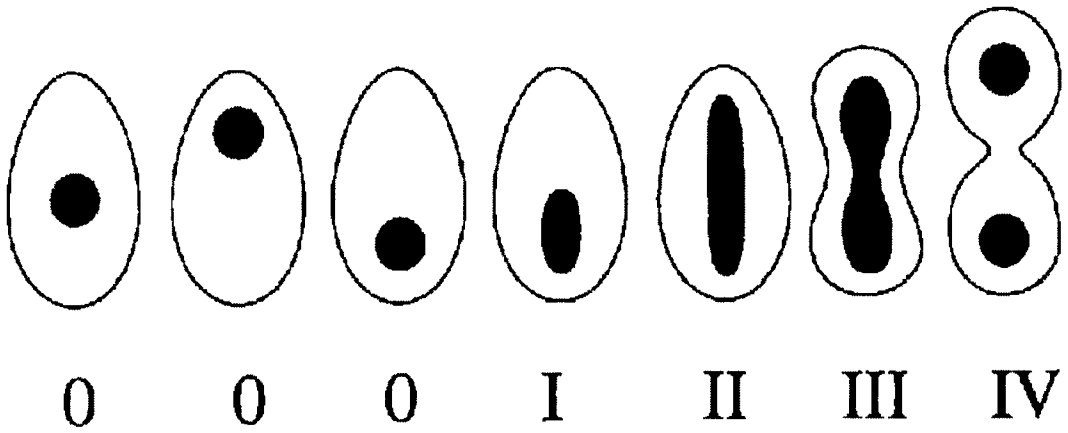

Fig. 9. A diagrammatic representation of the stages in macronuclear division of the cell *Tetrahymena thermophila.* Stage 0: The macronucleus is either centrally located or has migrated anterior or posterior as a prelude to elongation. Stage I: The macronucleus begins elongation from a posterior position within the cell. Stage II: The macronucleus is fully elongated and spans almost the entire length of the cell. Stage III: The elongated macronucleus is constricted at its midpoint, which coincides with the cell fission line. Stage IV: The constricted macronucleus is separated into two sub-nuclei.

Reproduced with permission of the copyright owner. Further reproduction prohibited without permission.

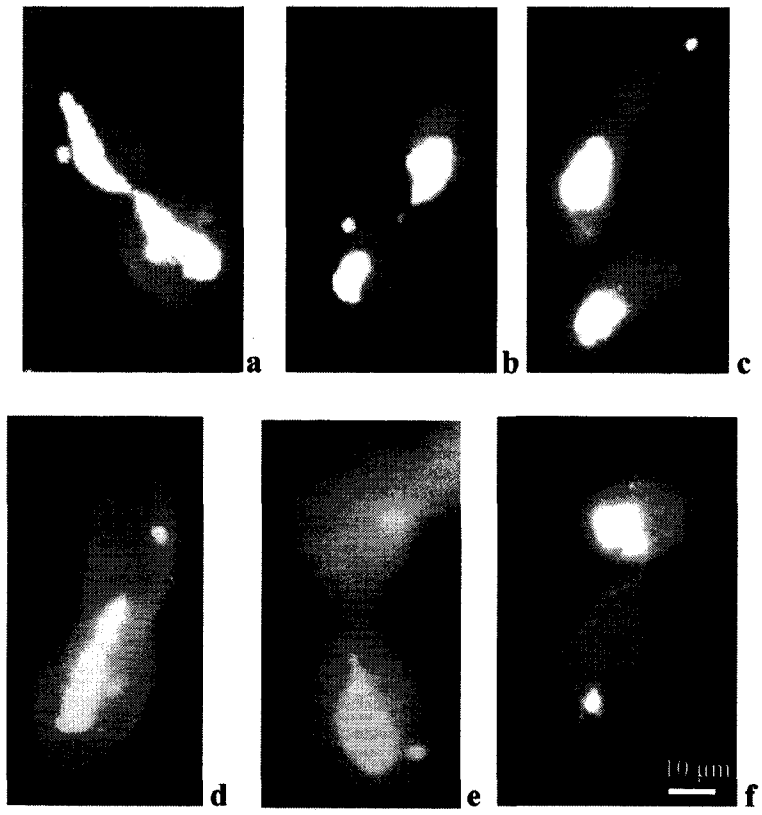

Fig. 10. DAPI-stained wild-type and *MYO1*-knockout (Δ*MYO1*) cells of *Tetrahymena thermophila* at 20 °C. A. Wild-type. Macronuclear elongation has been completed in this cell and constriction site (macronuclear midpoint) within the macronucleus coincides with the division furrow. **B.** Wild-type. Separation of the fully elongated and constricted macronucleus has been achieved prior to cytokinesis. **C.** Δ*MYO1*. The upper cell has not initiated macronuclear elongation, although a division furrow is present and micronuclear segregation has been completed. **D.** Δ*MYO1*. In this cell macronuclear elongation has been initiated but does not extend very far beyond the cell fission line. **E.** Δ*MYO1*. Although a deep furrow is present, the macronucleus has failed to elongate. **F.** Δ*MYO1*. Aberrant segregation of macronuclear DNA frequently produced amacronucleated cells. The amacronucleate condition is known to be lethal.

Reproduced with permission of the copyright owner. Further reproduction prohibited without permission.

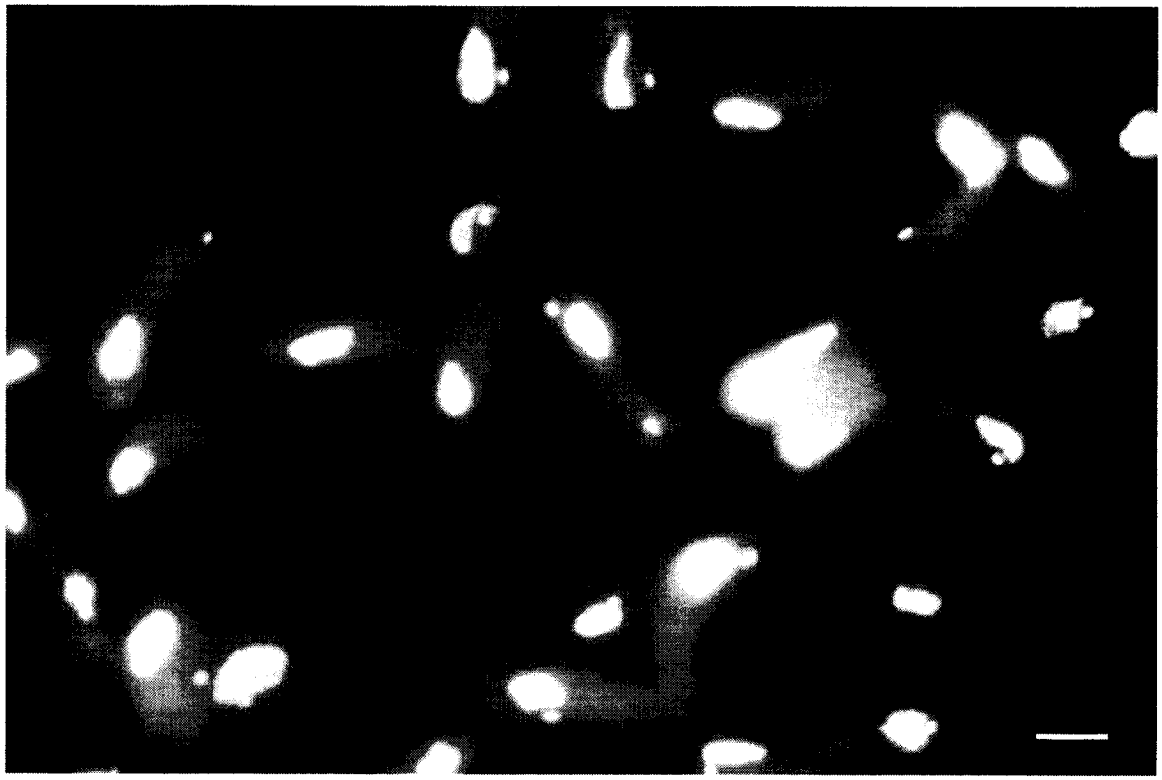

Fig. 11. DAPI-stained Δ*MYO1* cells of *Tetrahymena thermophila* from cultures maintained at 20 °C. In this micrograph, several cells possess macronuclei located to the posterior end of the cells and are partially elongated. Cells undergoing division are identified by the presence of a division furrow and micronuclei located at opposite ends of the cell. **Bar** = 20 μm.

Reproduced with permission of the copyright owner. Further reproduction prohibited without permission.

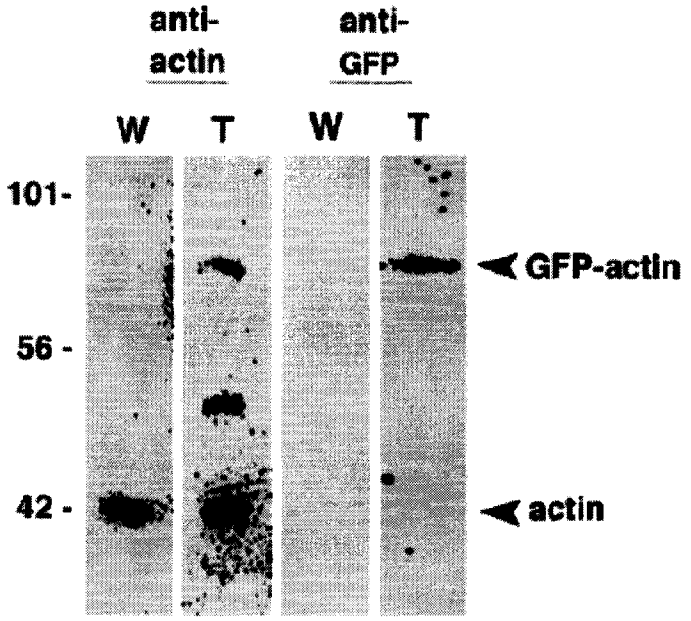

Fig. 12. Expression of actin and GFP-actin in *Tetrahymena*. Total lysate proteins from wild-type cells (W) and GFP-actin-transformed cells (T) were separated on 4%-12% DSD-PAGE gels. Standard immunoblot protocols were used with polyclonal anti-actin peptide and monoclonal anti-GFP antibodies. Molecular mass markers are on the left side of the figure.

Reproduced with permission of the copyright owner. Further reproduction prohibited without permission.

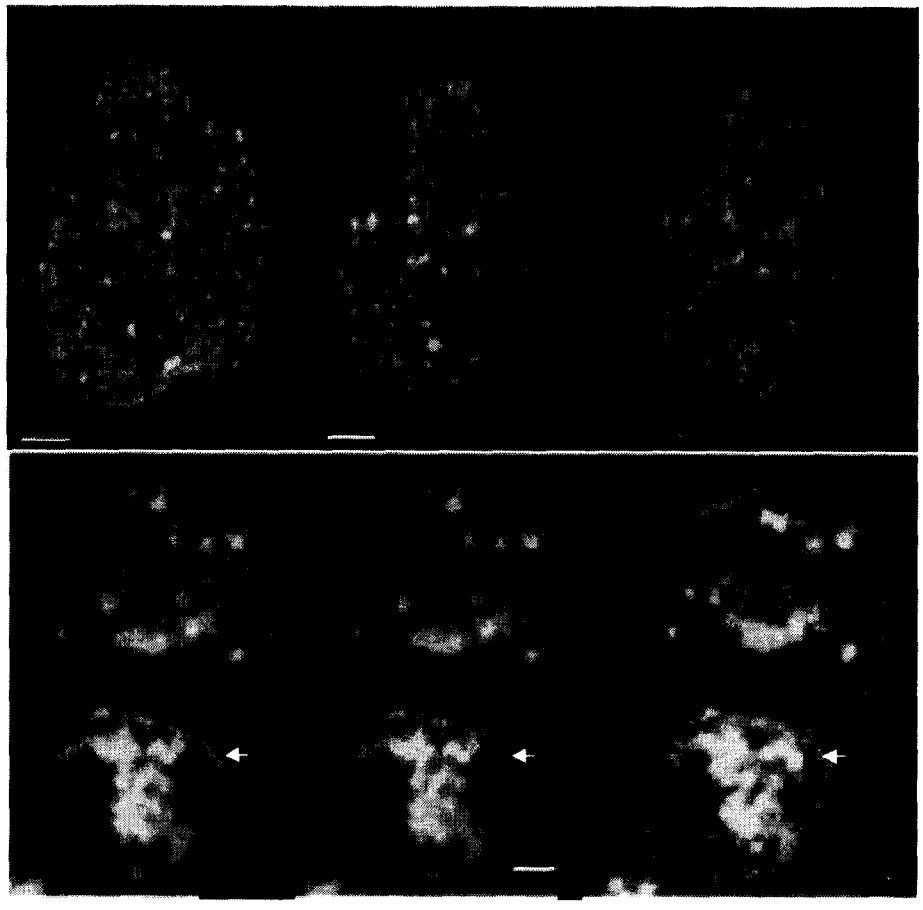

Fig. 13. Confocal microscope images of *Tetrahymena thermophila* expressing GFP-actin in vivo. Upper panel: Each picture is at a different focal plane through the cortex of the same living cell. The oral apparatus in this cell is not the plane of focus. **Lower panel:** Three focal scans through the subcortical region of a dividing cell. An encircling line of fluorescence denoting the position of the actin contractile ring is visible between the two subcells (arrowheads). The identity of the other fluorescent structures in the cell has not been determined. The unusual shape of the cell is due to the undulating movements of live cells embedded in agarose. **Bars:** Upper panel = 5 μm; Lower panel = 4 μm.

Reproduced with permission of the copyright owner. Further reproduction prohibited without permission.

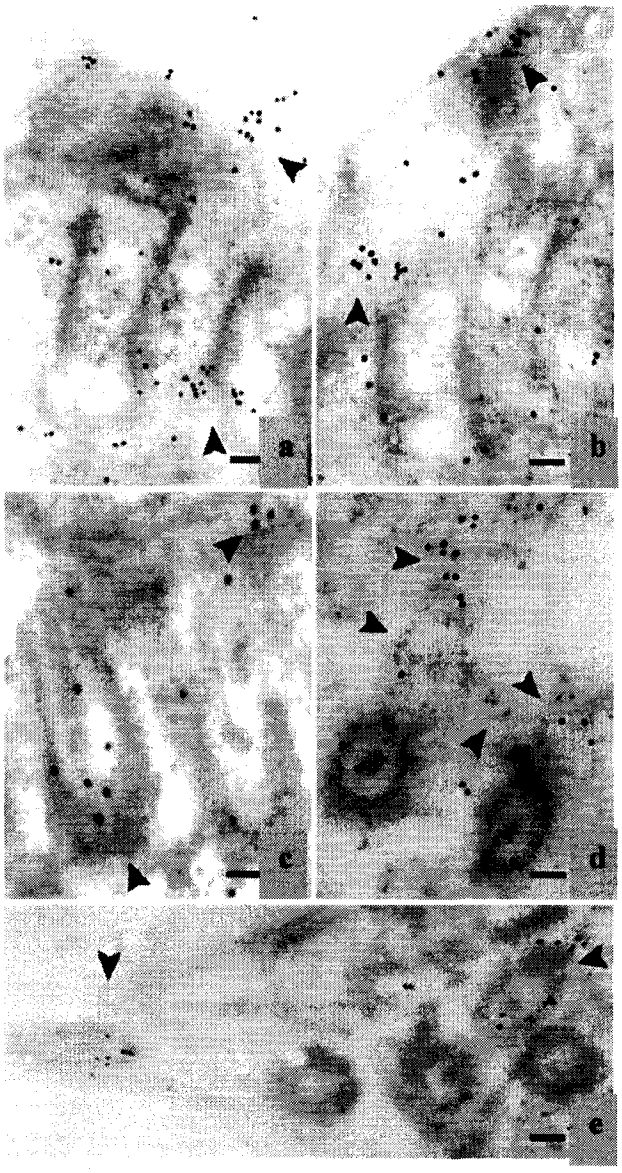

Fig. 14. Immunogold localization of actin. A, B. Anti-actin labeling in a cell expressing GFP actin. The three dense, vertically oriented structures in each figure are fibrillar partitions that form cage walls between adjacent basal bodies, which are not in the plane of section. The cage walls are labeled with small clusters of colloidal gold particles (arrowheads) at the proximal and distal ends. **Bar** = 0.13 μm. **C.** Anti-GFP labeling of basal bodies within the oral cavity of a call expressing GFP-actin. Colloidal gold particles (arrowheads) decorate the proximal region (base cage) of one basal body and the distal region of (cage top) of another basal body. **Bar** = 0.12 μm. **D.** Anti-actin labeling of basal bodies and associated fibrillar material (arrowhead) in a wild-type cell. **Bar** = 0.1 μm. **E.** Anti-GFP labeling of somatic basal bodies near the oral cavity in a GFP-actin strain. Two of the basal bodies (arrowheads) are labeled with colloidal gold. **Bar** = 0.1 μm.

Reproduced with permission of the copyright owner. Further reproduction prohibited without permission.

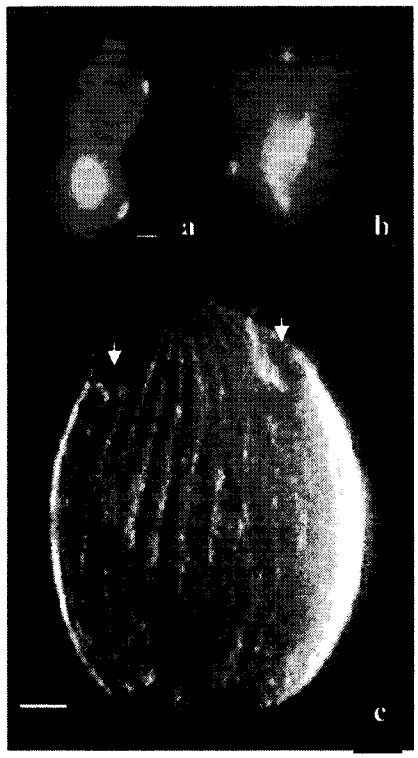

Fig. 15. Cells arrested in cytokinesis. A. DAPI-stained cell arrested in cytokinesis. Macronuclear elongation has failed to occur even though micronuclear division has been completed. **B.** A DAPI-stained, GFP-actin transformant doublet containing a macronucleus and two micronuclei. **C.** DIC image of a GFP-actin homopolar doublet formed from a cell arrested in cytokinesis. Arrowheads indicate the positions of the two oral apparatus. **Bars:** A, B = 10 μm; C = 5 μm.

Reproduced with permission of the copyright owner. Further reproduction prohibited without permission.

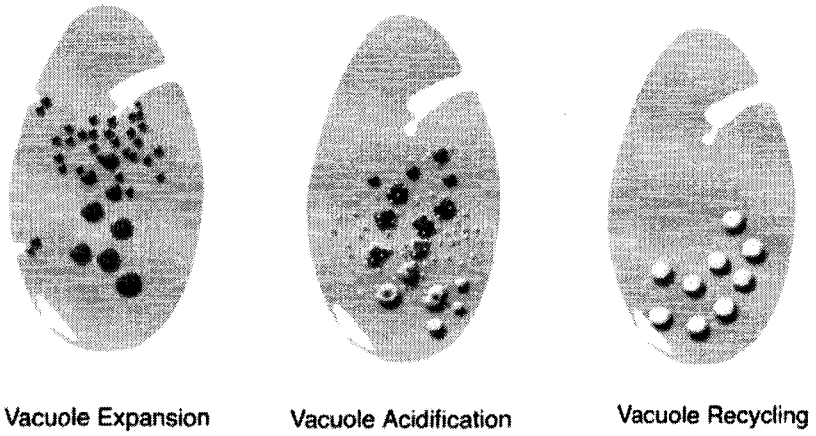

Fig. 16. A diagrammatic representation of major steps in the endocytic pathway in *Tetrahymena thermophila*. Membrane internalization occurs primarily at the oral apparatus, forming nascent food vacuoles shown in blue. Nascent vacuoles are rapidly expanded through a series of vacuole-vacuole fusions. The left margin of the first cartoon depicts other membrane invaginations known as parasomal sacs which may provide an alternate internalization pathway. Expanded endosomes fuse with lysosomes (white) and become acidified (yellow). Mature vacuole undergo egestion of vacuolar wastes and recycling of the vacuolar membrane at a specialized region of the cell's posterior known as the cytoproct.

Reproduced with permission of the copyright owner. Further reproduction prohibited without permission.

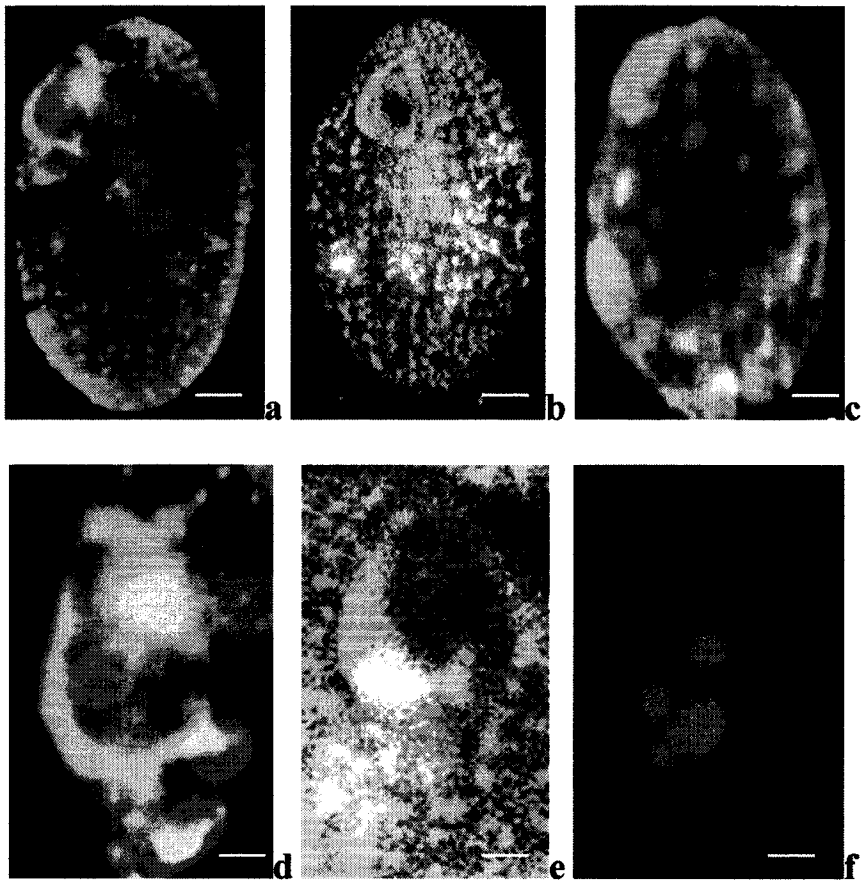

Fig. 17. Actin immunolocalization to food vacuoles and cortical structures in *Tetrahymena*. Cells were allowed to internalize 1 μm, red-fluorescent beads and subsequently imaged with confocal microscopy. **A.** Wild-type cell. The bright ring of fluorescence in the upper left margin of the cell is in the oral apparatus. **B.** A Δ*MYO1* (knockout) cell. **C.** A wild type cell in an early stage of division. A second oral apparatus (lower left margin) has developed for the posterior subcell but the division furrow has not formed. **D.** Enlarged view of wild-type buccal cavity. The yellow fluorescence result from regions of overlap of red (bead) and green (actin) fluorescence. **E.** An enlarged image of the buccal cavity in a Δ*MYO1* cell with bead containing vacuoles. **F.** A wild-type control cell in which anti-actin was omitted. **Bars:** A-C, F = 2 μm; D, E = 1 μm.

Reproduced with permission of the copyright owner. Further reproduction prohibited without permission.

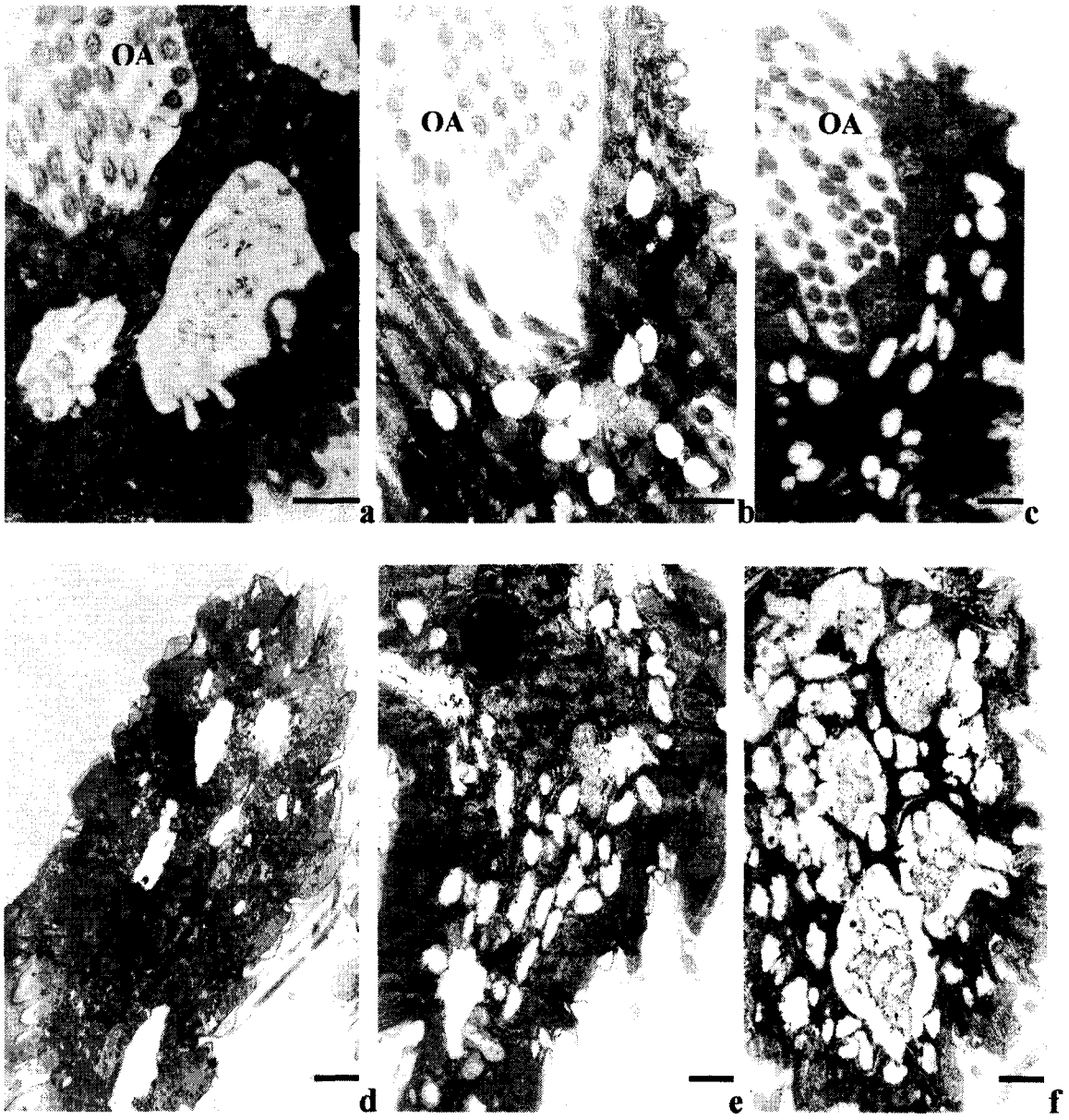

Fig. 18. Transmission electron micrographs showing vacuole morphology in wild-type and *ΔMYO1 Tetrahymena thermophila*. **A.** Wild-type. Electron-lucent nascent vacuoles located near the base of the oral apparatus (OA) appeared to have undergone rapid expansion. **B,C.** *ΔMYO1*. Nascent vacuoles of comparatively smaller size than wild-type accumulate in the oral region of the cell. In A-C, the buccal cavity of the oral apparatus is visible in the upper left and the axonemes of the oral cilia arrays are clearly distinguishable. **D.** Wild-type. Expanded vacuoles are distributed throughout the cell. **E.** *ΔMYO1*. Numerous smaller-sized vacuoles appear to congregate in the cell, though some expanded vacuoles are present. **F.** *ΔMYO1* showing vacuolar aggregates. Aggregates contain clusters of small vacuoles loosely connected by slender vacuolar extensions. **Bar** = 1.0 μm.

Reproduced with permission of the copyright owner. Further reproduction prohibited without permission.

A. Macronuclear Elongation

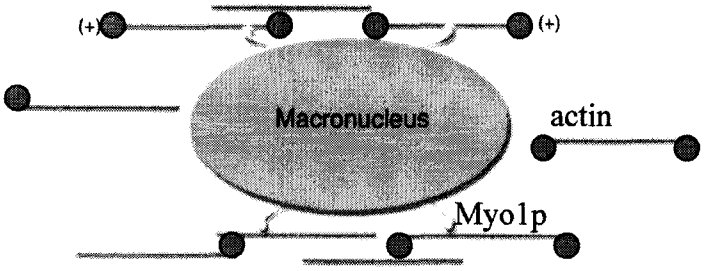

B. Vacuolar Fusion

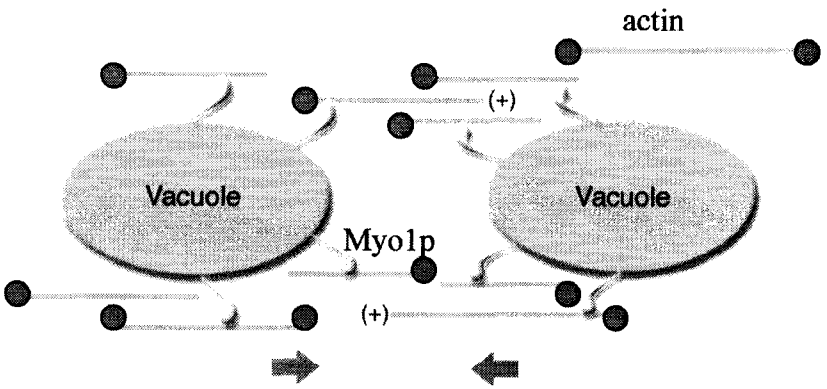

C. Myo1p-membrane interaction

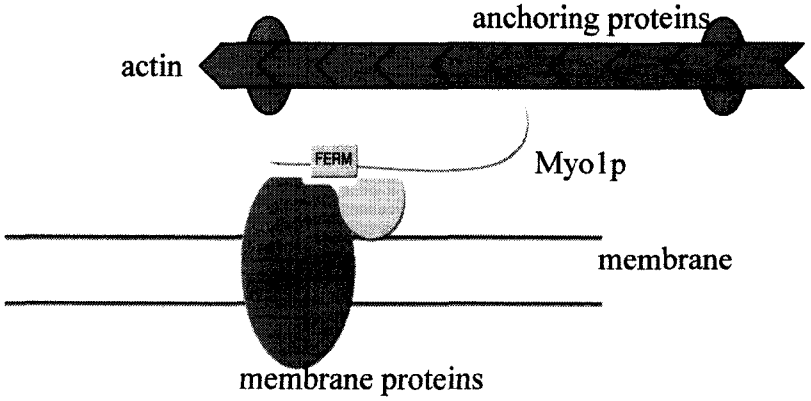

Fig. 19. Conjectural models of Myo1p function in macronuclear elongation and vacuolar fusion. Myo1p can act as a putative motor that can power the translocation of the macronucleus during elongation **(A)**. Similarly, the Myo1p-actin machinery could satisfy a translocatory requirement for efficient and rapid vacuole-vacuole fusions during early vacuolar expansion **(B)**. Directionality of movement can be established by the orientation of the microfilament arrays. Myolp can be localized to vacuolar and nuclear membrane via its FERM domain **(C)**. Red circles and ellipses represent anchor proteins that may participate in the organization and anchoring of the actin scaffold complex.

Reproduced with permission of the copyright owner. Further reproduction prohibited without permission.

References Cited

Adelman, M. R., and Taylor, E. W. (1969a). Isolation of an actomyosin-like protein complex from slime mould *Plasmodium* and the separation of the complex into actin- and myosin-like fractions. Biochemistry *8*, 4964-4975.

Adelman, M. R., and Taylor, E. W. (1969b). Further purification and characterization of slime mould myosin and slime mould actin. Biochemistry *8*, 4976-4988.

Aizawa, H., Sameshima, M., and Yahara, I. (1997). A green fluorescent protein-actin fusion protein dominantly inhibits cytokinesis, cell spreading, and locomotion in *Dictyostelium.* Cell Struct Funct *22*, 335-345.

Bement, W. M., and Mooseker, M. S. (1995). TEDS Rule: A molecular rationale for differential regulation of myosins by phosphorylation of the heavy chain head. Cell Motil Cytoskel *31*, 87-92.

Berg, J. S., Powell, B. C., and Cheney, R. E. (2001). A millenial myosin consensus. Mol Biol Cell *12*, 780-794.

Cassidy-Hanley, D., Bowen, J., Lee, J., Cole, E. S., Verplank, L. A., Gaertig, J., Gorovsky, M. A., and Bruns, P. A. (1997). Germline and somatic transformation of mating *Tetrahymena thermophila* by particle bombardment. Genetics *146*, 135-147.

Cleffman, G. (1980). Chromatin elimination and the genetic organization of the macronucleus in *Tetrahymena thermophila.* Chromosoma *78*, 313-325.

Cooke, R. (1993). Myosin structure: does the tail wag the dog? Curr Biol *9*, R773-R775.

Cope, M., Whisstock, J., Rayment, I., and Kendrick-Jones, J. (1996). Conservation within the myosin motor domain: implications for structure and function. Structure *4*, 969-978.

Corrie, J. E. (1999). Dynamic measurement of myosin light-chain-domain tilt and twist in muscle contraction. Nature *400*, 425-430.

Cupples, C. G., and Pearlman, R. E. (1986). Isolation and characteristics of the actin gene from *Tetrahymena thermophila.* Proc Nat Acad Sci USA *83*, 5160-5164.

Davis, L., Kuehl, M., and Battey, J. (1994). Basic Methods in Molecular Biology, 2nd edn (Norwalk, Connecticut, Appleton & Lange).

Doerder, F. P., and DeBault, L. E. (1978). Life cycle variations and regulation of macronuclear DNA content in *Tetrahymena.* Chromosoma *69*, 1-19.

Reproduced with permission of the copyright owner. Further reproduction prohibited without permission.

Engqvist-Goldstein, A., and Drubin, D. G. (2003). Actin assembly and endocytosis: from yeast to mammals. Annu Rev Cell Dev Biol *19*, 287-332.

Frankel, J. (1989). Pattern Formation. (New York, Oxford University Press).
Fujiu, K., and Numata, O. (2000). Reorganization of microtubules in the amitotically dividing macronucleus of *Tetrahymena*. Cell Motil Cytoskel *46*, 17-27.

Garces, J. A., Hoey, J. G., and Gavin, R. H. (1995). Putative myosin heavy and light chains in *Tetrahymena*: colocalization to the basal body-cage complex and association of the heavy chain with skeletal muscle actin filaments in vitro. J Cell Sci *80*, 659-663.

Garces, J. A., and Gavin, R.H. (1998). A PCR screen identifies a novel, unconventional myosin heavy chain gene (*MYO1*) in *Tetrahymena thermophila*. J Eukaryot (Euk) Microbiol, *45*, 252-259.

Gavin, R. H., Hoey, J. G., and Garces, J. A. (2000). Immunogold electron microscopy of *Tetrahymena*. In Methods in Cell Biology: *Tetrahymena thermophila*, D. J. Asai, and J. D. Forney, eds. (New York, Academic Press), pp. 333-343.

Geeves, M. A. (2002). Stretching the lever arm theory. Nature *415*, 129-131.

Goldman, Y. E. (1998). Wag the tail: Structural Dynamics of Actomyosin. Cell *93*, 1-4.

Gonda, K., Katoh, M., Hanyu, K., Watanabe, Y., and Numata, O. (1999). Ca^{2+}/calmodulin and p85 cooperatively regulate an initiation of cytokinesis in *Tetrahymena*. J Cell Sci *112*, 3619-3626.

Goodson, H. V., Anderson, B. L., Warrick, H. M., Pon, L. A., and Spudich, J. A. (1996). Synthetic lethality screen identifies a novel yeast myosin I gene (MYO5): myosin I protein are required for the polarization of the actin cytoskeleton. J Cell Biol *133*, 1277-1291.

Hirono, M., Kumagai, Y., Numata, O., and Watanabe, Y. (1989). Purification of actin reveals some unusual properties. Proc Nat Acad Sci USA *86*, 75-79.

Hirono, M., Nakamura, M., Tsunemoto, M., Yasuda, T., Obha, H., Numata, O., and Watanabe, Y. (1987). *Tetrahymena* actin: localization and possible biological roles of actin in *Tetrahymena* cells. J Biochem *102*, 537-545.

Hoey, J. G., and Gavin, R. H. (1992). Localization of actin in the *Tetrahymena* basal body cage complex. J Cell Sci *103*.

Jaeckel-Williams, R. (1978). Nuclear divisions with reduced numbers of microtubules in *Tetrahymena*. J Cell Sci *34*, 303-319.

Reproduced with permission of the copyright owner. Further reproduction prohibited without permission.

Kitajima, Y., and Thompson, G. A. (1977). Differentiation of food vacuolar membranes during endocytosis in *Tetrahymena*. J Cell Biol *75*, 436-445.

Lee, S., Wisniewski, J. C., Dentler, W. L., and Asai, D. J. (1999). Gene knockouts reveal separate functions for two cytoplasmic dyneins in *Tetrahymena thermophila*. Mol Biol Cell *10*.

Maniak, M. (2002). Conserved features of endocytosis in *Dictyostelium*. In Int. Rev. Cytol., K. Jeon, ed. (New York, Academic Press), pp. 257-287.

Maniak, M. (2003). Fusion and fission events inthe endocytic pathway of *Dictyostelium*. Traffic *4*, 1-5.

May, R. C., and Machesky, P. (2001). Phagocytosis and the actin cytoskeleton. J Cell Sci *114*, 1061-1078.

Metenier, G. (1984). Actin in *Tetrahymena paravorax*: ultrastructural localization of HMM-binding filaments in glycerinated cells. J Eukaryot (Euk) Microbiol, *31*, 205-215.

Mooseker, M. S., and Cheney, R. E. (1995). Unconventional myosins. Annu Rev Cell Dev Biol *11*, 633-675.

Neuhaus, E. M., and Soldati, T. (2000). Myosin I is involved in membrane recycling from early endosomes. J Cell Biol *150*, 1013-1026.

Nilsson, J. (1977). Fine structure and RNA synthesis of Tetrahymena during cytochalasin B inhibition of phagocytosis. JCell Sci *27*, 115-126.

Nilsson, J. (1999). Vanadate affects nuclear division and induces aberrantly-shaped cells during subsequent cytokinesis in*Tetrahymena*. J Eukaryot (Euk) Microbiol, *46*, 24-33.

Nilsson, J., and Van Deurs, B. (1983). Coated pits and pinocytosis in *Tetrahymena*. J Cell Sci *63*, 209-222.

Novak, K. D., Peterson, M. D., Reedy, M. C., and Titus, M. A. (1995). *Dictyostelium* myosin I double mutants exhibit conditional defects in pinocytosis. J Cell Biol *131*, 1205-1221.

Numata, O., and Gonda, K. (2001). Determination of division plane and organization of contractile ring in *Tetrahymena*. Cell Struct Funct *26*, 593-601.

Orias, E., Hamilton, E. P., and Orias, J. (2000). *Tetrahymena* as a laboratory organism: Useful strains, cell culture and cell line maintainence. In Methods in Cell Biology: *Tetrahymena thermophila*., D. J. Asai, and J. D. Forney, eds. (New York, Academic Press), pp. 291-312.

Reproduced with permission of the copyright owner. Further reproduction prohibited without permission.

Pollard, T. D., and Korn, E. D. (1971). *Acanthamoeba* myosin I. Isolation from *Acanthaomeba castellanii* of an enzyme similar to muscle myosin. J Biol Chem *248*, 4682-4690.

Qualmann, B., Kessels, M. M., and Kelly, R. B. (2000). Molecular links between endocytosis and the actin cytoskeleton. J Cell Biol *150*, F111-F116.

Rasmussen, L. (1976). Nutrient uptake in *Tetrahymena pyriformis*. Carlsberg Res Commun *4*, 143-167.

Rayment, I., Holden, H. M., Whittaker, M., Yohn, C. B., Lorenz, M., Holmes, K. C., and Milligan, R. A. (1993b). Structure of the actin myosin complex and its implications for muscle contraction. Science *261*, 58-65.

Rayment, I., Rypniewski, W. R., Schmidt-Base, K., Smith, R., Tomchick, D. R., Benning, M. M., Winkelmann, D. A., Wesenberg, G., and Holden, H. M. (1993a). Three-dimensional structure of myosin subfragment-1: a molecular motor. Science *261*, 50-57.

Sambrook, J., Fritsch, E. F., and Maniatis, T. (1989). Molecular Cloning. A Laboratory Manual, Vol 1-3, 2nd edn (Cold Spring Harbor, New York, Cold Spring Harbor Laboratory Press).

Sellers, J. R. (2000). Myosins: a diverse superfamily. Biochim Biophysacta *1496*, 3-22.

Soldati, T. (2003). Unconventional myosins, actin dynamics and endocytosis: a menage a trois. Traffic *4*, 358-366.

Someya, S., Gonda, K., Kanzawa, N., and Numata, O. (2000). *Tetrahymena* myosin: the cloning of six myosin genes in *Tetrahymena thermophila*. Mol Biol Cell *11:S*, 376a.

Sorkin, A. (2000). The endocytosis machinery. J Cell Sci *113*, 4375-4376.

Spudich, J. A. (1994). How molecular motors work. Nature *372*, 515-518.

Stuart, K. R., and Cole, E. S. (2000). Nuclear and cytoskeletal fluoresence microscopy techniques. In Methods in Cell Biology: *Tetrahymena thermophila.*, D. J. Asai, and J. D. Forney, eds. (New York, Academic Press), pp. 291-312.

Tanka, H., Homma, K., Hikikoshi, I., Katayama, E., Ikebe, R., Saito, J., Yanagida, T., and Ikebe, M. (2002). The motor domain determines the large step of myosin-V. Nature *415*, 192-195.

Taunton, J., Rowning, B. A., Coughlin, M. L., Wu, M., Moon, R. T., Mitchson, T. J., and Larabell, C. A. (2000). Actin dependent propulsion of endosomes and lysosomes by recruitment of N-WASP. J Cell Biol *148*, 519-530.

Reproduced with permission of the copyright owner. Further reproduction prohibited without permission.

Titus, M. A. (2000a). The role of unconventional myosins in *Dictyostelium* endocytosis. J Eukaryot (Euk) Microbiol, *47*, 191-196.

Titus, M. A. (2000b). Getting to the point with myosin VI. Curr Biol *10*, R294-R297.

Titus, M. A. (2003). An unconventional myosin essential for the initiation of *Dictyostelium* development. Mol Biol Cell *14:S*, 181a.

Turkewitz, A., Chilcoat, N. D., Haadad, A., and Verbsky, J. W. (2000). Regulated protein secretion in Tetrahymena thermophila. In Methods in Cell Biology: *Tetrahymena thermophila.*, D. J. Asai, and J. D. Forney, eds. (New York, Academic Press), pp. 347-362.

Tuxworth, R. I., and Titus, M. A. (2000). Unconventional myosins: achors in the membrane traffic relay. Traffic *1*, 11-18.

Weibel, E. R., Kistler, G. S., and Scherle, W. F. (1966). Practical stereological methods for morphometric cytology. J Eukaryot (Euk) Microbiol, *33*, 352-358.

Weihing, R. R., and Korn, E. D. (1971). Acanthamoeba actin. Isolation and properties. Biochemistry *10*, 596-600.

Williams, N. E. (1986). The nature and organization of filaments in the oral apparatus of *Tetrahymena.* J Eukaryot (Euk) Microbiol, *33*.

Worthington, D. H., Salamone, M., and Nachtwey, D. S. (1976). Nucleo-cytoplasmic ratio requirements for initiation of DNA replication and fission in *Tetrahymena*. Cell Tissue Kinet *9*, 119-130.

Zackroff, R. V., and Hufnagel, L. A. (1998). Relative potencies of different cytochalasins for the inhibition of phagocytosis in ciliates. J Eukaryot (Euk) Microbiol, *45*, 397-403.

Zackroff, R. V., and Hufnagel, L. A. (2002). Induction of anti-drug resistance in *Tetrahymena.* J Eukaryot (Euk) Microbiol, *49*, 475-477.

Zhang, F., Southwick, F. S., and Purich, D. L. (2002). Actin-based phagosome motility. Cell Motil Cytoskel *53*, 81-88.

Reproduced with permission of the copyright owner. Further reproduction prohibited without permission.